Design of Intermittently Operated Reverse Osmosis System and Membrane Coatings for Enhanced Fouling Mitigation

BY

BRANDON TRUONG

A THESIS SUBMITTED TO THE FACULTY OF GRADUATE STUDIES IN PARTIAL FULFILLMENT OF THE REQUIREMENTS FOR THE DEGREE OF MASTER OF APPLIED SCIENCE

GRADUATE PROGRAM IN MECHANICAL ENGINEERING
YORK UNIVERSITY
TORONTO, ONTARIO

December 2022

Abstract

Access to potable water is becoming an increasingly important issue, especially in communities residing in remote, off-grid locations. The use of solar powered reverse osmosis systems has been shown to be a viable solution to delivering clean drinking water. There is a need to improve the fouling resistance of the membranes to reduce costs, maintain water quality, and keep water output reliable. Membrane coatings have been shown to enhance antifouling properties, but more research is required.

A lab-scale reverse osmosis (RO) system is developed to enable testing and monitoring of intermittent water treatment processes. Multiple sensors used to measure water quality and permeate flow were incorporated inline to gather data in real time. Membrane coating technology used to improve treatment performance through enhanced antifouling properties was studied. Several coating possibilities were considered for criteria such as: cost, antifouling & anti-scaling properties, and water output quality.

Acknowledgements

I am very thankful for everyone in the Freire-Gormaly group at York University. My Masters program would not be successful without them. The guidance and support by Prof. Marina Freire-Gormaly was greatly appreciated. Her kindness and eagerness to help was always apparent, and I hope to see the lab grow from the humble beginnings from when I joined the group.

Thank you to members of the department who helped me with the electronics involved: Norman Nicholls, Armando Azevedo, Florin Alexandru from Mechanical Engineering. Thank you to my colleagues Liam Horrigan, Kishon Winston, and Arma Khan for the help on building my experimental setup.

I am thankful for my parents and family members who supported me along the way. All my friends who continued to push me forward and provide the social support is greatly appreciated.

Table of Contents

List of Tables

List of Figures

Chapter 1

1 Introduction

1.1 Motivation

In 2020, over 770 million people lack access to improved or basic drinking water services [1]. Global water usage increases by roughly 1% per year, as agricultural and energy production demands also increase [2]. There are large gaps in accessibility and quality of drinking water between urban and rural areas in water stressed regions [1]. As a result, people turn to untreated water sources such as rivers, ponds, or wells which potentially contain contaminants such as bacteria, pollutants, or excessive chemicals [1]. These contaminants compromise the taste and nutritional value of the water, and present a risk of infection and disease to those who ingest the water [3]. Many rural communities lacking potable water are also situated away from centralized electricity grids. Thus, these communities rely instead on diesel generators and renewable energy [4], [5]. These rural communities are located in regions that often correlate with higher solar irradiance levels, as shown in Figure 1. In these regions, there is adequate solar power that can be harnessed via photovoltaic cells to provide clean, affordable electricity. Alternative energy sources have been implemented for off-grid power supply for water treatment plants such as wind powered reverse osmosis (RO) desalination [6], [7], solar thermal desalination [8]–[10], and solar photovoltaic reverse osmosis (PVRO) desalination [11]–[15].

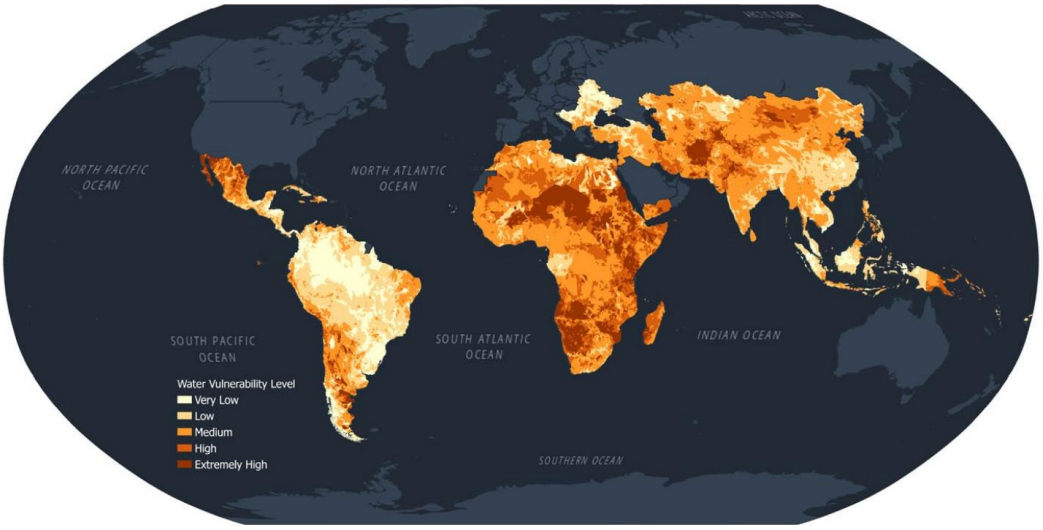

Figure 1: The world map highlighting regions of high or extreme water vulnerability [16].

Membrane-based desalination is considered an industry leader in water desalination technology since its rise in the 21st century [17], [18]. Of the currently available technologies, reverse osmosis is the leading technology, comprising of over 77% of the total desalination capacity worldwide [19]. Provision of RO desalinated water is highest by countries in water stressed regions, with the Middle East, Northern Africa, and Asia-Pacific housing the majority of large and extra-large plants (by capacity, Mm^3/day) [19]. Desalination is also an attractive option due to its independence from factors such as droughts, river systems, and reservoir levels. The process of desalination involves removing salts and other contaminants from brackish water or seawater to produce drinking water. Reducing the level of dissolved minerals to concentrations of <500 mg/L total dissolved solids (TDS) qualifies the water as drinkable in Canada, as well as many other countries (Table 1)[20].

Table 1. Water salinity ranges determined by total dissolved solids (TDS)

Water Type	Salinity (mg/L of TDS)
Potable water	<500
Fresh water	50 – 500
Brackish water	1,000 – 10,000
Seawater	30,000 – 45,000

Despite the growing interest in membrane-based desalination solutions, the high energetic requirements to operate an RO plant is a point of contention for many regions that seek to address water scarcity. Energy requirements of an RO plant is influenced by factors such as membrane permeability and feed water chemistry. These factors in turn influence the potential for energy recovery and the percent recovery of clean drinking water from the feed water [21]. Energetic requirements have dropped significantly as RO has become more prevalent, from 6 kWh/m^3 in 1980 to less than 2 kWh/m^3 in 2008 [22]. Although this improvement in efficiency has been achieved, the energy requirement remains substantial for low-income residents. With this energy requirement, community operated off-grid RO plants are faced with two choices: 1) invest in costly energy storage options, or 2) operate the RO system intermittently based upon demand and/or energy availability [23], [24]. Intermittent operations can lower the initial capital costs associated with batteries and procuring continuous power, but this operation mode comes at the cost of enhanced fouling rates of the membrane used for desalination [25].

1.2 Problem Statement

Reliable solutions to water scarcity are becoming increasingly important as the global population rises, specifically in water-stressed regions. Intermittently operated RO plants currently suffer from enhanced fouling rates due to the downtime when power is not available. Scaling due to deposition and crystallization of salts and fouling from bacterial growth on the surface of the membrane reduces membrane permeability, increases energy requirements, and reduces salt rejection. The cost per cubic meter of water increases as the RO plant ages, due to maintenance and replacements of the membrane. There is an urgent need for the development of membrane technology to better combat fouling and increase drinking water outputs of reverse osmosis desalination plants. Currently, commercial membrane coatings designed to address fouling do not consider intermittent operation during testing. Membrane coatings have been studied and published extensively, however there are few practical applications that have been actualized at the commercial scale. There is also a gap in the literature pertaining to whether membrane coatings are effective when using complex water matrices, involving a variety of salts and other biological materials.

1.3 Research Objectives

The goal of this research is to investigate the performance of membrane nanocoatings for intermittently operated RO plants. By determining the fouling mechanisms during intermittent operation with coated membranes, better understanding of the viability of coatings and their applications can be achieved. A clearer understanding of how coatings interact with a mixture of foulants will also be investigated by using water samples designed to mimic real brackish water. In intermittently operated RO plants, the cycle of uptime and downtime is scheduled to coincide

with the availability of solar energy throughout the day. The experimental findings are to be analyzed to assess the extent of fouling. This can then be compared with pristine (uncoated) membranes or other coated membranes. The following objectives were set out to accomplish these goals:

1. Development of a lab-scale crossflow reverse osmosis system allowing for implementation of membrane coatings.
2. Conduct experimentation to characterize fouling rates for intermittent operation with and without membrane coatings.
3. Determine fouling behaviour of membrane coatings with feed water mimicking brackish water sources.

1.4 Research Scope

Within this thesis, the described research conducted focuses on the development of the lab-scale RO system. The system is described in detail and was developed to enable various experimental endeavours, even beyond the scope of this research. Additionally, the experimentation involving a polydopamine coated membrane is outlined. Initial tests were performed with the pristine membrane to establish a basis for the coated membrane experimentation that would occur subsequently. The experimental water used consisted of distilled water provided by the department, and lab-grade chemicals were prepared to adjust the mineral content of the water to desired concentrations of brackish water. Of the three objectives mentioned in 1.3, objective 1 was completed during the duration of this project. Due to COVID-19 restrictions, lab and university access was severely limited, hindering the progress of the project. Timelines for completing objective 1 was stretched due to supplier delays caused by the pandemic.

1.5 Thesis Organization

The thesis is presented in four chapters. The first chapter covers the introduction, problem statement, research goals and objectives. Chapter two is an overview of the background and a literature review of renewable energy RO systems, membrane fouling mechanisms, and membrane coating technologies. Chapter three outlines the experimental system that was built, and the methodology behind how data is collected and analyzed. This chapter also reports preliminary data using distilled water to illustrate membrane pre-compression and system equilibrium. The fourth chapter provides a conclusion and directions for future work.

Chapter 2

2 Background and Literature Review

2.1 Reverse Osmosis Desalination

There are a variety of methods to obtain clean, potable water such as multi-effect distillation, multi-stage flash, filtration (micro, ultra, nano, reverse osmosis), chemical treatment, flocculation, and disinfection [26], [27]. Reverse osmosis falls under the filtration category, utilizing a semipermeable membrane to separate ions, particulates, and large undesired molecules from water [28]. By doing so, separation of harmful chemicals, excess salts, and bacteria results in water that meets drinking water safety standards [2], [6]. Reverse osmosis is unique among filtration techniques as it works by overcoming the natural osmotic pressure of water. An applied pressure is used to drive the separation process and push water through the semipermeable membrane, which is an energy intensive process to produce permeate – the pure, ion-free water (Figure 2). Concentrate (or brine) is collected as the waste product. The semipermeable membrane acts as the filter in this process as a barrier for ions and contaminants, due to its small pore size of <0.5 nm [29]. In contrast to other membrane filtration methods such as micro, ultra, and nanofiltration, reverse osmosis boasts the smallest pore size and thus the highest selectivity [29]. Reverse osmosis is the preeminent choice for desalination due to the lower energy cost per cubic meter (m^3) of permeate water produced, modularity, and the RO process being non-thermal. RO fresh drinking water production globally from seawater is over 30.6 million m^3/day, while brackish water is 17.8 million m^3/day [30]. There is significant drop-off in water production globally from

multi-stage flash distillation, the next leading desalination technology at 15.3 million m^3/day from seawater [30].

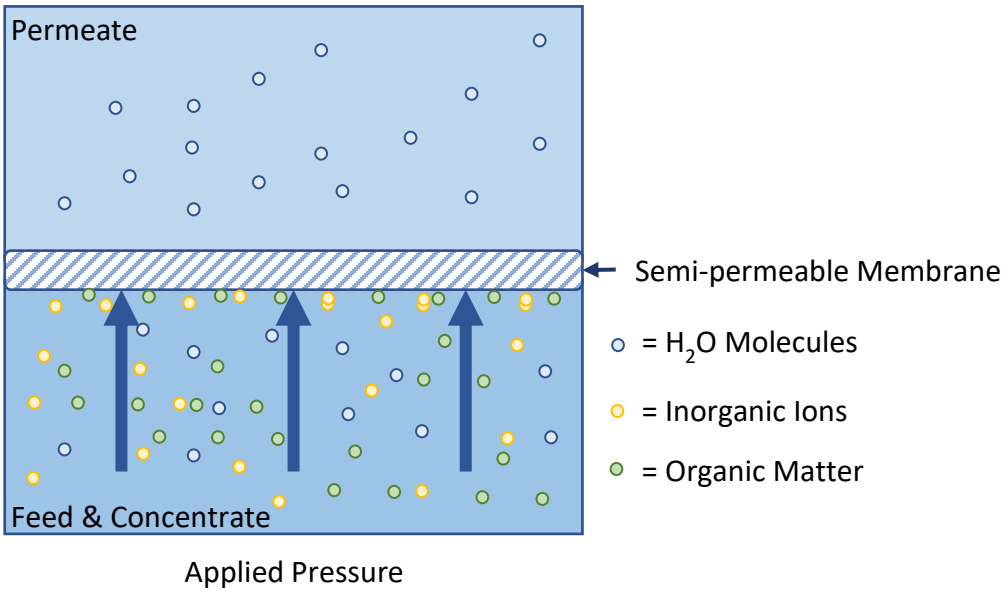

Figure 2. Simplified diagram of a crossflow RO cell. An applied pressure counteracts the natural forward osmotic pressure, allowing water (but not other molecules) to pass through the semi-permeable membrane.

Conventional reverse osmosis plants operate continuously at a large scale to deliver enough drinking water to support municipalities. Extra-large and large RO plants make up over 70% of the world's global RO capacity, whereas medium and small plants account for the remaining share, as seen in Table 2 [30]. The water price associated with RO plants has no correlation to size, but rather the infrastructure, price of energy, and other auxiliary factors. To this end, employing large or small RO plants dependent on situational needs is possible.

Table 2. Reverse osmosis plants according to size and share of global capacity.

Size	**Capacity (m^3/day)**	**% Global Capacity**
Small (S)	<1000	4 %
Medium (M)	1000 - 10,000	24 %
Large (L)	10,000 - 50,000	33 %
Extra-Large (XL)	>50,000	39 %

2.1.1 Renewable Powered Reverse Osmosis

Branching from conventional RO plants are renewable energy reverse osmosis plants. There is increasing interest in combining water treatment with renewable energy to address the carbon footprint of current desalination plants [22]. Energy demands of RO systems hover around 2-4 kWh/m^3 [31], [32]. This number can vary depending on the feed water salinity, membrane permeability, and whether or not energy recovery devices are utilized [30]–[32]. This figure can be put into perspective when compared to MSF and MED distillation technologies, which require 10-16 kWh/m^3 and 5-6 kWh/m^3 respectively. The lower energy requirements mean currently less efficient technologies such as photovoltaic cells can deliver enough energy throughout the day to operate the system. There have been proposed RO projects [14], [33], [34] and small-scale implementations for PVRO in South American and African nations [12], [13], [35]. There are challenges with implementation however, as waste (in the form of brine) disposal and ongoing maintenance of the plant can be difficult to manage for any RO plant, let alone smaller, isolated plants which are in remote or off-grid communities [15]. Nonetheless, there are many studies looking at improving the feasibility of PVRO systems from multiple angles such as economic [36], energy recovery [37] and daily output [38].

2.1.2 Intermittently Operated Reverse Osmosis Systems

When considering renewable energy in the context of RO systems, it is important to highlight the intermittent nature of wind, solar, or other suggested renewable energy sources. To reduce capital costs and logistical issues, eliminating batteries for energy storage in favour of intermittently operated systems coupled with large water tanks has been utilized [39]–[41]. Doing so means desalination can only occur during the hours with available energy, such as during daylight hours. This also means consideration for the location of implementation such that the solar irradiation levels are adequate to supply power for the system to run as often as possible. With this method, the system runs with a low carbon footprint, and may be operated outside of a centralized electricity grid, which is advantageous in locations without access to conventional electricity. Figure 3 shows a schematic of the main components involved in a PVRO system. The distinct disadvantage of intermittently run systems is the enhanced membrane fouling rate during shutdown periods [39], [40], [42].

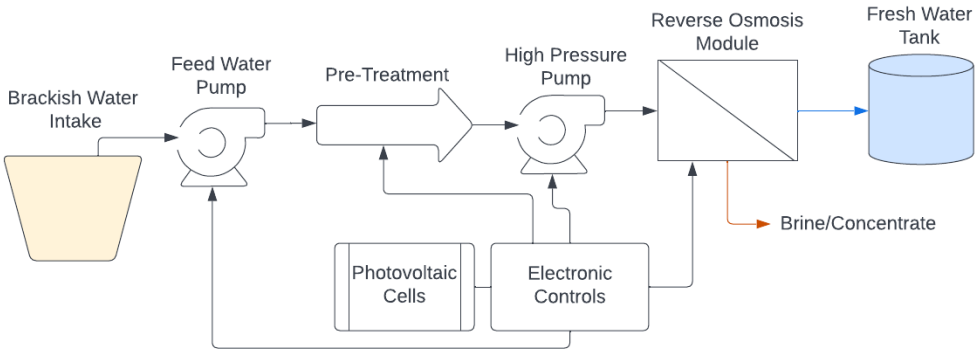

Figure 3: Basic schematic for a PVRO system operating intermittently without energy storage.

2.2 Reverse Osmosis Membrane Fouling

RO membranes are fabricated with materials to ensure high salt rejection, water permeability, and stability to chemicals, physical scouring, and thermal conditions. To this end, aromatic polyamide (PA) thin film composite (TFC) membranes dominate the current commercial RO membrane market [43]. Unfortunately, TFC membranes suffer from its vulnerability to fouling as well as chlorine attack, which would otherwise eliminate foulants in the feed water [43], [44]. Although membrane fouling is enhanced to a degree in intermittently operated systems, membrane fouling is a major issue throughout all reverse osmosis systems, and is the topic of extensive research [45]–[49]. There are multiple avenues in which fouling may occur, depending on the constituents existing in the feed water. Biofouling, inorganic scaling, organic fouling, and colloidal fouling are the four categories of deposited material onto the membrane surface [45], [47], [49]. Membrane fouling is detrimental to the RO system due to increased pressure required to maintain permeate output (and thus energy requirements) and costs associated with replacing, cleaning, and maintenance of the membrane modules [46], [50]. Increased pressure is due to the increased mass transfer, as foulants accumulate at the membrane surface. Fouling is one of the main barriers to

implementing RO desalination and is therefore an area extensively studied. Described below are the individual categories of fouling, scenarios in which they occur, and the fouling mechanisms.

2.2.1 Biofouling and Organic Fouling

Various microorganisms that may exist within the feed water are responsible for the proliferation of biofouling on the membrane surface. Bacterial contaminants such as Corynebacterium and Pseudomonas, fungi such as Penicillium and Trichoderma, or yeast such as Candida were found in fouled membranes used in northern Europe [44]. In other water purification processes, chlorination would be employed as part of a multi-step process to remove these biological contaminants [47]. This however is not a strong long-term solution, as degradation of 99.9% of bacteria still leaves a small amount that may grow on the membrane surface. Breakdown of other acids and molecules such as humic acids by chlorination can also provide nutrients to surviving bacteria. Lastly, chlorination is not a viable strategy for pre-treatment in RO, as conventional membrane materials are vulnerable to the chemicals used in chlorination [43]. The costly workaround to this is de-chlorination prior to filtration, which adds an additional step to the overall treatment process.

Biofouling occurs in a multistage process and has been extensively studied [49], [51], [52]. First, deposition of the bacteria and organics onto the membrane surface occurs as the RO system operates. Microbial cells and other organic material may adsorb onto the surface of the wet membrane, creating a favourable environment for growth. The extent to which cells attach onto the surface depends on the surface characteristics of the membrane, such as roughness, hydrophilicity, and polarity [47]. Microorganisms that colonize the surface then grow and multiply, creating a biofilm consisting of aggregated cells and extracellular polymeric substance (EPS). The EPS acts as a barrier made of organic material (such as polysaccharides, proteins, glycoproteins,

lipoproteins) around the cells, thus allowing continual growth and protection [50], [53]. Finally, shear forces from the RO process detaches part of the colony from itself, dispersing the cells onto another location of the membrane surface, and so begins another cycle of biofilm formation [54].

Polyamide membranes used in RO are not entirely flat at the surface, but have small, bumpy ridges that allows small molecules to deposit onto the surface. These ridges and crevices serve as sanctuaries for bacterial growth, as shear forces from the feed water are unable to scour the bacteria out. The biofilm of bacterial cells acts as an additional layer in which water must permeate through, reducing the efficiency of the filtration process. A transmembrane pressure drop occurs, resulting in permeate flux decline [55]. The EPS also has hydrated gel-like properties which increase the hydraulic resistance, impeding water movement through the membrane [56], [57]. This also affects the salt rejection of the membrane, by creating a stable zone for salts to accumulate, leading to enhanced concentration polarization [55], [58]. Biofouling is an ongoing issue and continues to contribute to degraded membranes.

2.2.2 Inorganic Scaling

Another branch of contaminants that may be deposited onto the surface of membranes are inorganic salts. Commonly found in brackish and seawater are various hydrated forms of $CaCO_3$, $CaSO_4$, and silica, which can cause blockage of the membrane surface [49]. As with biofouling, permeate flux decline and decreased salt rejection also occur with increased scaling. Scaling occurs due to concentration polarization (CP), a mechanism which occurs naturally as the RO system operates.

The phenomenon known as concentration polarization occurs naturally as the RO system operates. The dissolved particles in the feed water aggregate at the membrane surface, resulting in

higher concentrations compared to the bulk feed water supply [59]. This results in increased salt passage through the membrane and plays a key role in scale formation. Salts can crystallize on the surface of the membrane, due to the favourable conditions of high solute concentration and presence of a surface in which crystals may nucleate. This nucleation is aided again by the roughness of membrane surfaces.

2.2.3 Intermittently Operated RO Membrane Fouling Studies

Due to the favourable membrane surface chemistry, fouling occurs gradually over time as contaminants deposit and grow on the surface. This is exacerbated in intermittent operation due to the long downtime during periods of low energy input. When comparing continuous RO to intermittent RO, the normalized permeate decline is greater for intermittent operation [40]. Addition of a rinse with permeate water prior to shutdown at the end of each day improved the permeability considerably, as the salt concentration and nutrient supply for biological growth would be reduced [40]. In all cases, membrane autopsies using scanning electron microscopy (SEM) and X-ray electron dispersive spectroscopy (EDS) showed varying levels of biofilm growth and small to medium sized crystals on the membrane surface. Osmotic suck-back, a mechanism whereby a small force resulting in flow reversal, occurs when the system is turned off, as a sort of forward osmosis. When the system then turns back on, turbulence at the membrane surface due to pressure changes can induce loosening of the accumulated foulants. These mechanisms provided minor contributions to reducing concentration polarization but is limited by the surface area exposure to the permeate side of the membrane [40]. As such, these mechanisms are much less pronounced in spiral-wound membrane modules.

Currently, antiscalants additives and manual removal of salts and nutrients (by permeate water rinsing) at the membrane surface are relied upon to allow intermittent RO systems to operate

without severe permeability decline. These methods add costs, resources and time that can act as barriers of entry for small-scale RO system implementation. Using part of the permeate water obtained means less daily output, and usage of antiscalants is dependent on the feed water chemistry to be used. Over the short-term, these methods are sufficient, but it is unknown whether long-term permeability recovery is sustainable. Addressing membrane fouling by implementing preventative technologies on the membrane itself instead of pre-treatment (anti-scalant) and membrane treatment with permeate rinsing after operation may provide distinct advantages.

2.3 Membrane Coating Antifouling Technologies

Among several strategies, surface modified membranes via nanocoatings have been studied extensively to improve the antifouling properties of membranes for conventional continuously operated RO plants. By altering the surface of membranes, enhanced properties which serve to reduce fouling and permeate decline can be achieved. There are a variety of coatings reported in the literature, ranging from metal nanoparticles (NPs) to organic polymers [60], [61]. The coating materials may be attached to the membrane surface via physical and chemical treatments such as adsorption, plasma treatment, chemical coupling, or grafting [62]–[64]. Physical bonds through hydrogen bonding, Van der Waals forces, and electrostatic interactions are relatively weak, and thus not highly suitable for adhering coatings for long-term operation.

2.3.3 Membrane Properties

There are several properties which can influence the performance of membranes. Surface chemistry is the most unique, as it is comprised of the chemical structure of the material making up the membrane itself [60]. Functional groups containing oxygen atoms such as carboxylic acids and hydroxyls provide enhanced hydrophilicity, allowing water to form a barrier on the surface of

the membrane. Carboxylated nanodiamonds incorporated into a polyvinylidene fluoride membrane and polyvinyl alcohol incorporated into a polyaromatic TFC membrane was shown to enhance hydrophilicity and antifouling performance [65], [66]. Biocidal agents such as Ag, Cu, graphene oxide (GO), or antibiotics have also been incorporated into membrane modification [67]–[69]. Hydrophilicity is an important parameter which can be measured most simply via the water contact angle (WCA) between the surface and a water droplet. WCA of $0° < \theta < 90°$ denotes a hydrophilic surface, because of hydrogen bonding between oxygen-containing functional groups and water molecules. Formation of a hydration layer acts as a preventative barrier to scalants and foulants from depositing on the membrane surface itself [60], [65]. There is merit in measurement of hydrophilicity through interfacial Gibbs free energy [70], however this is uncommon in the membrane literature and therefore will not be a topic of discussion. It is unclear whether hydrophilic coatings can be employed for long-term use and is a topic for further research.

The surface charge of membranes is another property which influences fouling rates of the membrane surface. Electrostatic interactions between functional groups, inorganic salts, organic material, and bacterial cells play a pivotal role in fouling rates. There is debate in the literature around whether more negatively charged surfaces are more resistant to fouling than less charged surfaces [71]–[73]. Composition of the feed water was variable in the studies [71]–[73], and it appears the desirable charge for a given water source must be determined on a case-by-case basis.

Surface morphology, or the roughness of the surface can influence fouling rates severely, owing to the propensity of foulant deposition within crevices of the membrane. It has been shown that rougher surfaces correlated with higher colloidal fouling in RO membranes, regardless of physical or chemical operating conditions [74], [75]. Foulants enjoy the protection that is offered

by the ridges and valley structure present in rough surfaces. Membrane coatings reducing roughness is therefore desirable, but not always attainable [68].

The most common membrane used in industry are PA TFC membranes (Figure 4), which contain a thin PA layer (<200 nm), micro-porous substrate layer (~40 μm), and non-woven fabric support layer (~120 μm) [76]. Three distinct modification methods have been utilized in the literature: substrate modification pre, during, and post interfacial polymerization [60], [77]. Focus will be set on post interfacial polymerization, as preparing TFC membranes in-lab is beyond the scope of this study. Instead, commercially purchased membranes can be modified. Conveniently, surface-modified membranes enable the most direct testing for the coating of interest, due to its tunable concentration and accessibility by being at the top of the membrane rather than incorporated within the top layer.

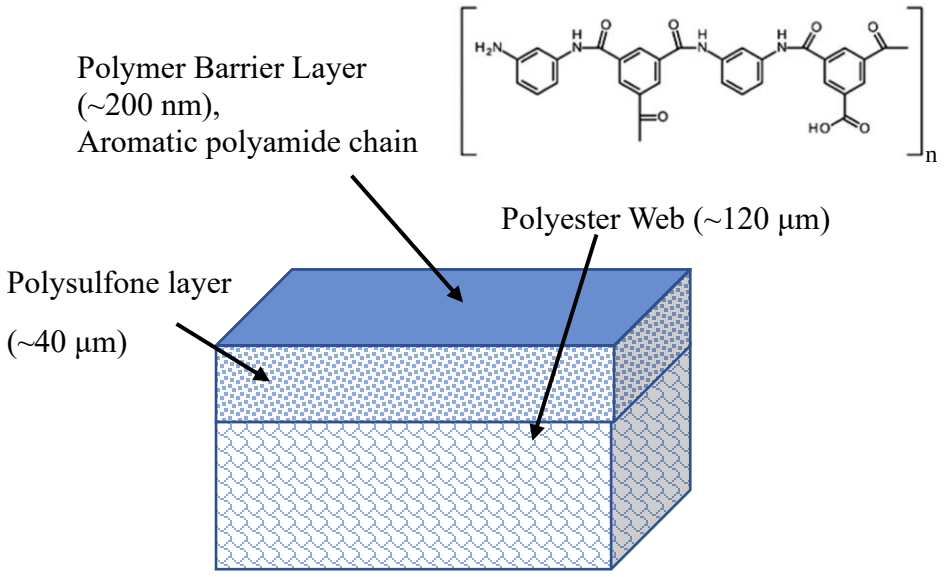

Figure 4. the chemical structure of the thin PA layer, layered on top of the polysulfone and polyesther layers [76].

2.3.4 Inorganic Nanoparticles

As mentioned previously, many inorganic nanomaterials such as Ag, Cu, TiO_2, GO, $BaSO_4$, and CuO carry biocidal properties and thus may provide enhanced biofouling mitigation [60]. Without large sacrifices to permeate flux and salt rejection, researchers have reported enhanced biofouling resistance using a variety of in-situ generation methods [68], [78]. In previous years, issues surrounding the affordability of metal nanoparticles was of concern, thus pushing the search for inexpensive ways to load the nanoparticles onto the surface of the membrane. Processes reported [60] have been effective in antifouling performance, however the relatively smooth surface of RO membranes (compared to UF or MF), combined with weak bonding between nanoparticles and the membrane, means that long-term operation remains impracticable, ultimately holding back their potential as cost-saving measures in RO desalination. Catalytic oxidation reactions with H_2O_2 (a chemical cleaning agent for RO membranes) also damages the membrane surface, hindering the long-term viability of this coating type [68], [78], [79].

Dissolution of the nanoparticles is dependent on the chemistry of the feed water, as well as hydrodynamic conditions present at the membrane surface [78], [79]. It is currently challenging to implement long-lasting, stable inorganic coatings without hindering permeate flux to some degree.

2.3.5 Organic Polymers

There are several categories of polymer chain modified membranes: hydrophilic polymers, zwitterionic polymers, biomimetic polydopamine, and other polymers [60]. These types of coatings are preferred over inorganic nanomaterials due to the higher compatibility between polymer chains, allowing for more stability. The PA membrane surface contains carboxylic acid and amide groups, which allows for surface grafting. Surface grafting is the process whereby polymer chains are added to the surface of the membrane through a variety of methods such as UV, redox, chemical vapour deposition, cationic, anionic, free radical, or enzymatic mechanisms [60]. The common theme of polymeric membranes involves hydrophilicity enhancement to better facilitate formation of a hydration layer to combat fouling [60]. A hydrophilic polymer such as poly (ethylene glycol) (PEG) is a neutrally charged, long flexible chain that can prevent adsorption of hydrophobic, organic molecules and mineral scalants [80]. PEG is effective at preventing organic protein adsorption, but also susceptible to oxidation by O_2 and transition metal ions, and are thus limited in complex water matrices [81].

Zwitterionic molecules containing positively and negatively charged atoms are found in many biological systems such as the phospholipid bilayer of the cell membrane. While PEG forms a hydration layer through hydrogen bonding, zwitterions such as poly (sulfobetaine methacrylate), or pSBMA, form hydration layers through electrostatic interactions which are stronger and enable more water molecules to bind [70], [82]. For foulants to penetrate this stronger hydration barrier, more energy is required (ΔG is increased). The structure of the hydration layer also resembles free

water molecules more closely than PEG, resulting in more stability. The structure of zwitterions is also conducive to steric hindrance. Due to this, compression of the polymer chains by foulants is energetically unfavoured, resulting in recovery of the swelled (by water) state and prevents foulants from contacting the membrane surface [70].

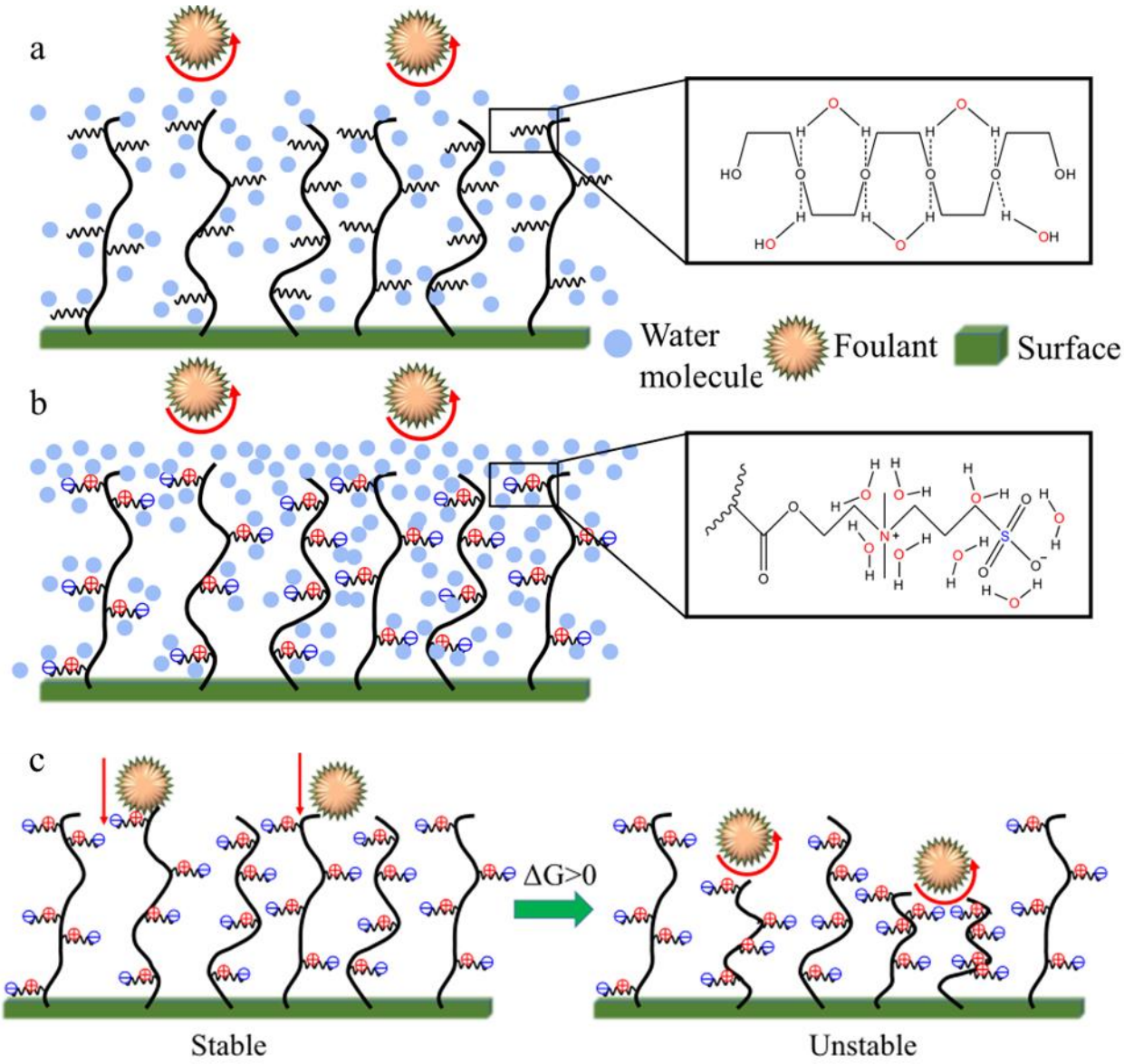

Figure 5. (a) PEG hydrogen bonding prevents foulants from penetrating the membrane surface. (b) Zwitterionic pSBMA molecules interact with more water molecules through electrostatic interaction [70]. (c) During compression by foulants, the coating becomes unstable. Recovery of the stable state by rejecting foulants protects the membrane surface [70].

2.4 Summary and Research Gaps

The literature review has shown that there are plenty of reported membrane coatings and coating modification methods to target every variety of foulants in feed water. The inorganic

nanoparticle class of coatings offer strong biofouling protection, high costs, and preparation methods have already been employed in previous research and industry applications. The organic polymer class of membrane coatings can be summarized as a low-cost, highly robust group. The antifouling properties are reported for a variety of foulants from inorganic scalants to biological contaminants. The salt rejection and permeate flux performance is hindered to an extent, however this is the case with all coatings studied in the literature. The environmental risks are minimized due to the lack of dangerous constituents, with coatings being free of metals that could leech into the permeate over time. A combination of organic polymers with inorganic nanoparticles have been reported to improve salt rejection, antifouling, and antimicrobial performance, with Ag and Cu being the primary metals incorporated, however more research is needed to assess long-term efficacy before adoption [83]–[85].

Membrane nanocoatings present an interesting avenue into improving RO performance by addressing its main drawback of membrane fouling. Optimization of the membrane surface to combat specific foulants has led to numerous reported performance enhancements. The introduction of coatings inevitably causes mass transfer resistance. This necessitates a balance of antifouling performance and flux reduction to be established based upon maintenance cost, energy cost, and water output requirements. When considering intermittently operated remote PVRO systems, the longevity and energy costs are even more pronounced factors to consider. The relatively recent interest in intermittently operated PVRO systems is apparent, as there are no coating studies mentioning or incorporating intermittent processes during operation.

Chapter 3

3 Experimental Systems and Methods

3.1 Introduction

In this chapter, the experimental system that was built for the purpose of RO membrane research is described. The various components involved in building the system include the plumbing from the feed tank, through the high-pressure pump and RO modules, and recirculation. As each component was sourced individually, there is also a system to control the pump via LabVIEW and an Arduino microcontroller. Sensors and other data collecting parts are connected through this system as well, allowing for real-time monitoring of parameters such as pressure and flowrate. The key components are outlined in the schematic diagram below (Figure 6). This is a simplified version of the actual experimental system, which is detailed in Section 3.2.

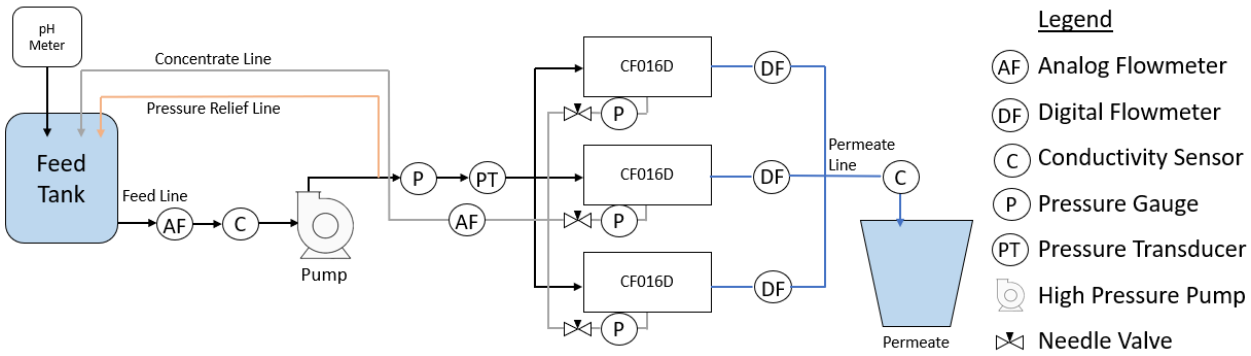

Figure 6. A schematic diagram of the RO system.

3.2 Lab-Scale RO System

The RO system constructed utilizes Sterlitech CF016 crossflow filtration units in triplicate. The active membrane area is 20.6 cm^2, allowing for minimal product, expenses, and time when conducting experimentation (Figure 7). Each component of the system was chosen with membrane coating experimentation prioritized; thus, a smaller active membrane area facilitates simple application and membrane autopsy. Described below are the parts involved following from the feed tank, through the system, and recirculating back as concentrate.

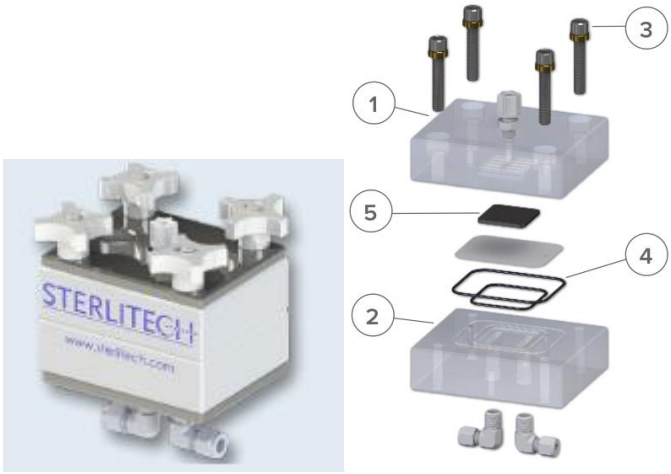

Figure 7. (Left) The CF016 Innovator crossflow filtration unit assembled. (Right) Individual parts of the cell, including membrane sheet.

3.2.1 Feed Flow Setup

To begin, the 50-gallon (189 L) feed tank acts as the reservoir from which water is drawn and recirculated to and from the system. The tank is elevated slightly from the pump such that the inlet is gravity fed into the pump (Figure 8). There is an on/off ball valve leading to plastic hosing throughout the inlet side of the pump. Before reaching the pump inlet, there is a feed flowmeter (FPR302, Omega) and a conductivity sensor to measure the flowrate and salt concentration of the feed water. These parameters may be cross-referenced with the recirculation & permeate flowrate, and the permeate conductivity. The pressure at this part of the system is ambient (~101.35 kPa), with a minor suction from the pump inlet during operation that allows the water to flow smoothly through. Once the water passes through the high-pressure pump (M03-E, Hydracell), the pressure of the system is elevated to over 2758 kPa. After the pump outlet, all piping and hosing used are stainless steel, high-pressure components which can withstand up to 4137 kPa.

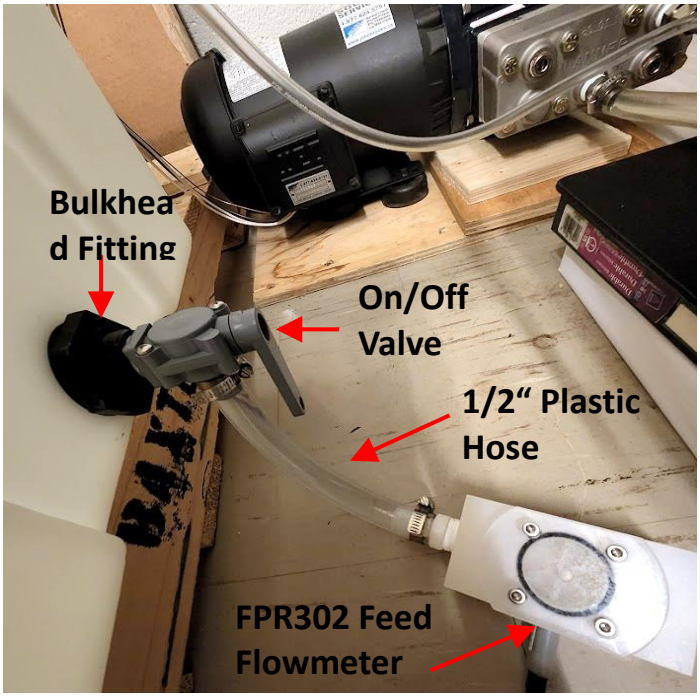

Figure 8. The feed tank placed on a pallet. The grey valve is fitted onto the bulkhead fitting on the bottom of the tank.

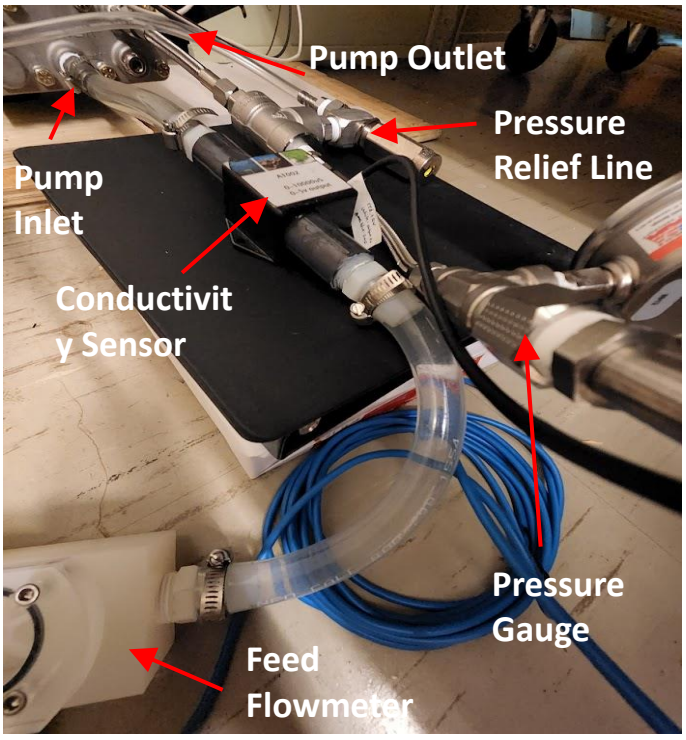

Figure 9. The pump inlet and outlet plumbing.

The pressure relief line next to the outlet of the pump acts as the bypass for water to flow should the internal pressure exceed the calibrated amount (Figure 9). The pressure threshold can be altered by the valve itself, and the pressure gauge downstream is used to accurately read the current pressure of the feed line. After the pressure gauge, the flexible steel hose moves up from ground level to the table, where it is supported by a wooden block and metal straps. The hosing is changed to 1/4" steel tubing, due to the plumbing compatibility with the RO modules (Figure 10). Figure 11 shows the remaining feed flow line, where the steel pipe is first met with a pressure transducer attached to a tee to electronically measure pressure readings. The flow then splits through a cross to three RO modules, where crossflow filtration occurs.

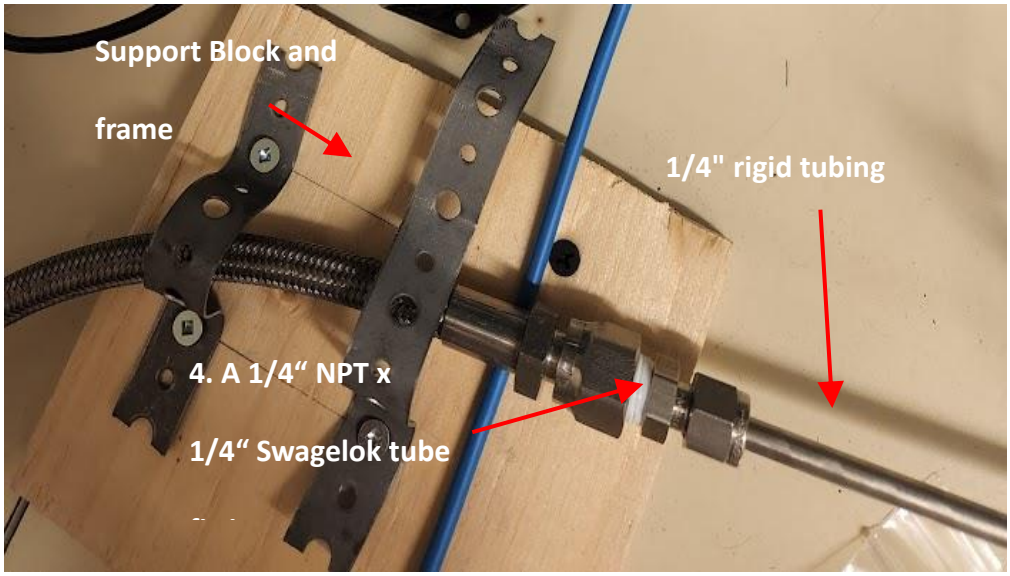

Figure 10. The feed water moves up to the table, through the steel hosing, through the steel pipe.

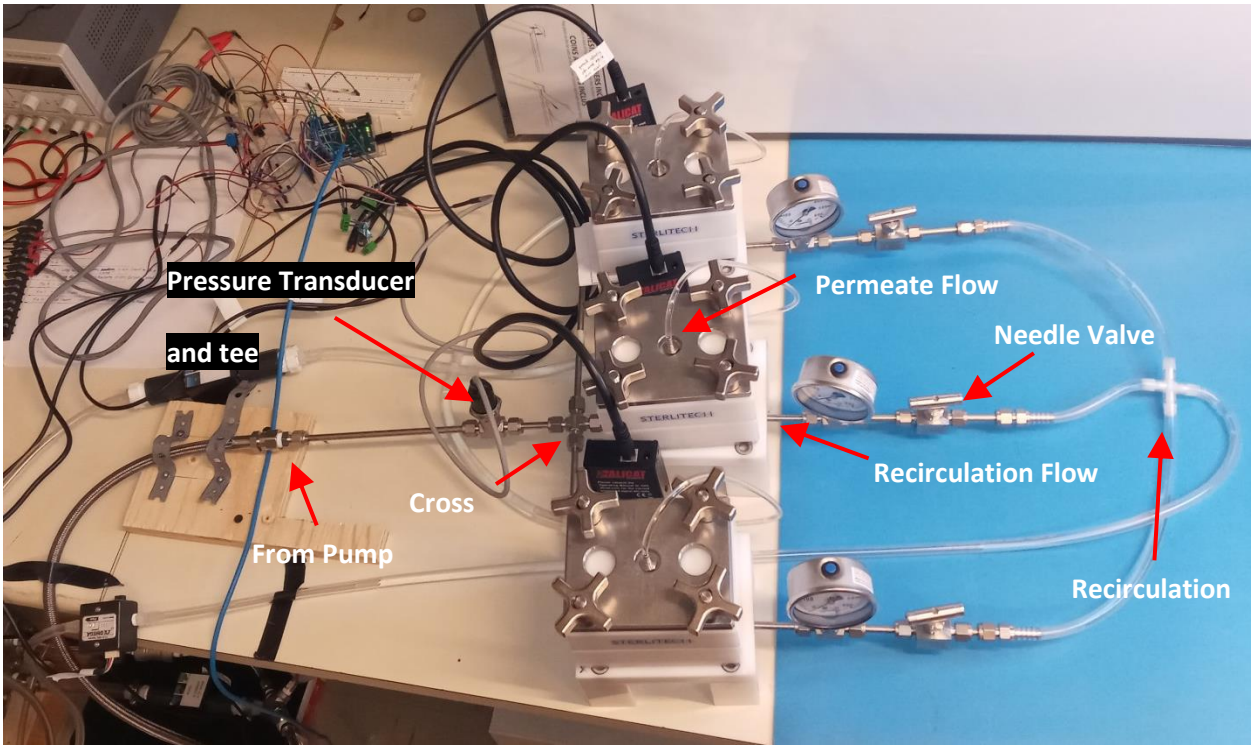

Figure 11. The RO system including three RO crossflow modules.

3.2.2 Permeate and Recirculation Setup

Figure 12 shows the view from below the RO modules, where the feed and recirculation flow through the bottom of the module. The permeate flows through the membrane out the top, in the clear plastic hose. The permeate can be collected or recirculated, after the flowrate (L-10CCM-D/5V, Alicat) is measured. Measurement of the flowrate at the permeate line is one of the main parameters to analyze when assessing the fouling over time. At the recirculation side, the brine is collected and its flow measured (FLR1011, Omega), before recirculating (Figure 11).

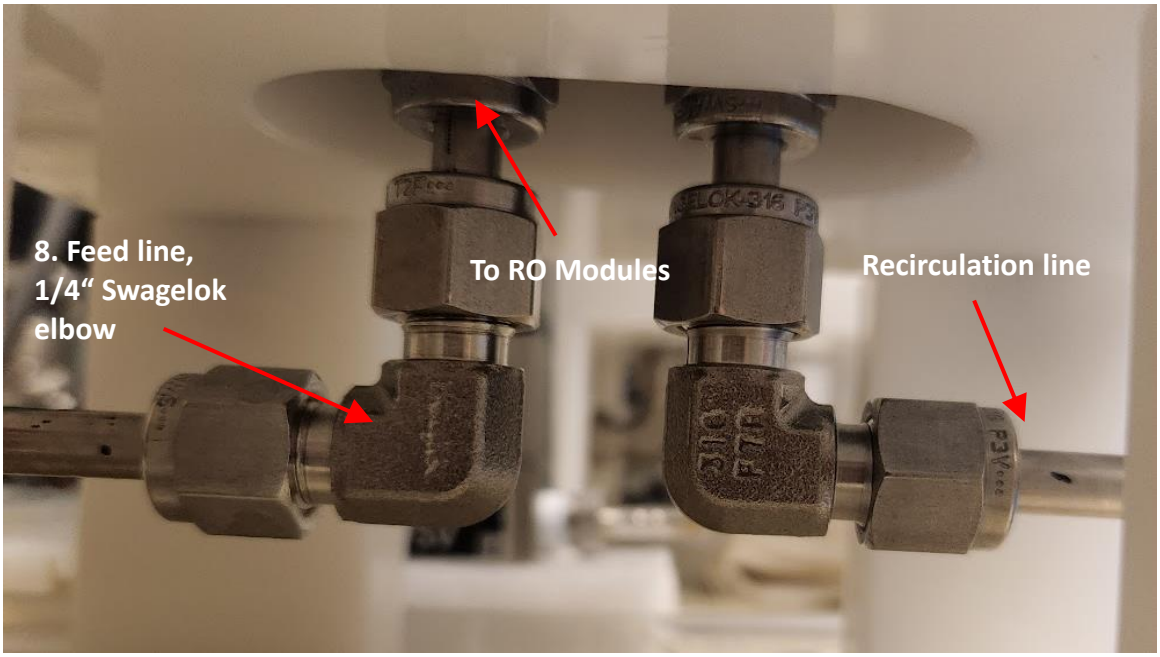

Figure 12. Underneath the RO modules where the feed and recirculation lines are located.

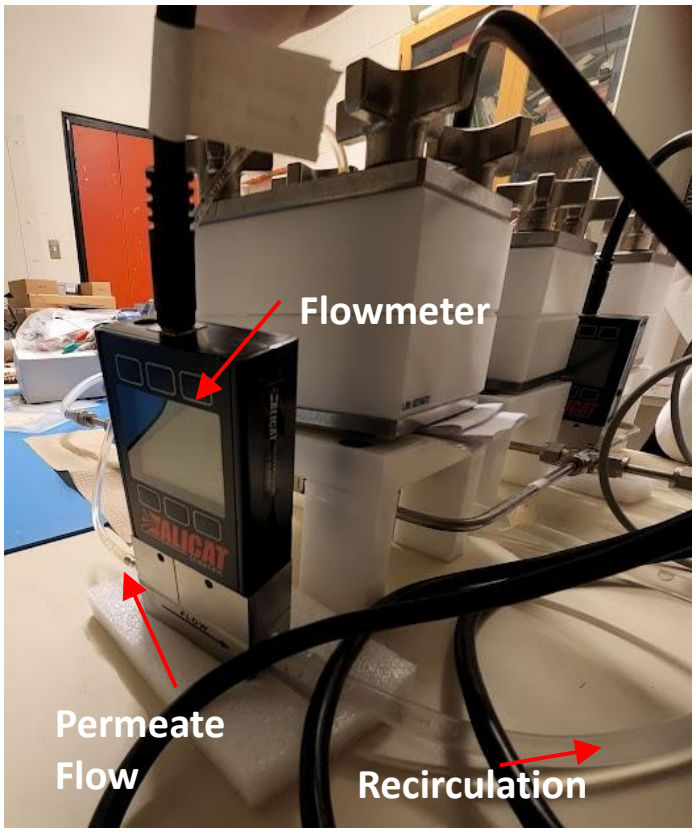

Figure 13. The permeate line, where flux is measured.

3.3 Electronics and Data Collection System

This section covers the overall setup involving all electrical components. There was significant consideration on how the sensors and the data collection system could be designed to operate reliably. The pump and variable frequency drive (VFD) is described, alongside all the flowmeters and conductivity sensors. The Arduino microcontroller and LabVIEW UI are also described in this section.

3.3.1 Sensors

All the sensors are capable of continuous monitoring of the system, to allow for experiments that can run for long periods of time (8 hours or longer). There are several flowmeters used to assess the conditions of the system and are used to ensure that the system is running as intended. Each flowmeter is slightly different, suited to the flowrate and application of the water line it is located on (Table 3).

Table 3. Summary of the flowmeters used in the system.

Flowmeter	**Location**	**Purpose**
FPR302 (Omega)	Feed line	• Ensure feed line is flowing without disruption • Calculate flowrate of entire system and cross reference with permeate and recirculation flows
FLR1011 (Omega)	Recirculation	• Analog flowmeter to measure flux decline • Flowrate across membrane surface measurement
L-10CCM-D/5V (Alicat Scientific)	Permeate	• Flux decline measurement • Permeate flowrate of individual modules • Cross reference with other module flowrates for averaged results

The pressure transducer (MLH500PSL01A, Honeywell) is used to electronically measure the pressure of the system at the feed line. This is important to ensure that reverse osmosis is occurring at the desired pressure reading. The calibration for the transducer is performed with the pressure gauge upstream of the transducer, and both should read the same pressure throughout the specified range of 0-3147 kPa. The conductivity sensor (eC/pH Transmitters, USA) indirectly measures the salt content of the solution (ranging from 0-10,000 μS) by the water's ability to pass an electrical current. The feed water, with its higher salt content, should have a greater conductivity than the permeate water, which has been filtered and should display conductivity nearer to distilled water. The measurement is done inline, through the feed and permeate lines, but can also be measured externally.

To power the sensors themselves, an external DC power supply is utilized (72-8335A, Tenma). 11.5 VDC power is provided to all the sensors which require this voltage rating. Meanwhile, the Arduino also provides 5 VDC output, which was used for other devices. The VFD can output 24 VDC, however this was not necessary nor relied upon due to the interference that could occur with the highly important pump operation. The pH and temperature of the water is measured externally, as these parameters are stable and do not cause significant alterations to performance in the controlled environment of the system.

3.3.2 Pump and VFD

The high pressure forward displacement pump (M-03E, Hydracell) is the primary workhorse to enable the high pressures required for reverse osmosis (Figure 14). To control the motor's frequency and thus the rpm, a variable frequency drive is employed (

Figure 15. The VFD with connections identified. L1, L3, Ground from the Transformer powers the VFD and pump. UVW To Pump are the connections for the power. The control connections

are connected to the Arduino microcontroller.). The VFD (Commander C200, Nidec) is connected directly to the pump and can either be controlled directly on the VFD interface, or through an external controller (more detail is provided on this external controller in Section 3.3.3). Due to the high-power requirements for the VFD and pump, a transformer is used to deliver 240 V, which is connected directly to the VFD.

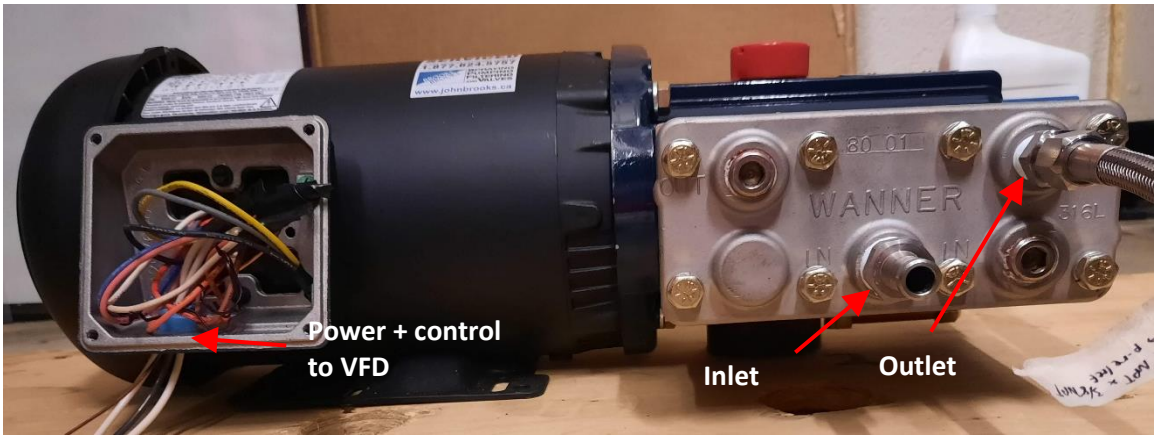

Figure 14. The pump is supported on a wooden slab underneath rubber stoppers to absorb vibrations.

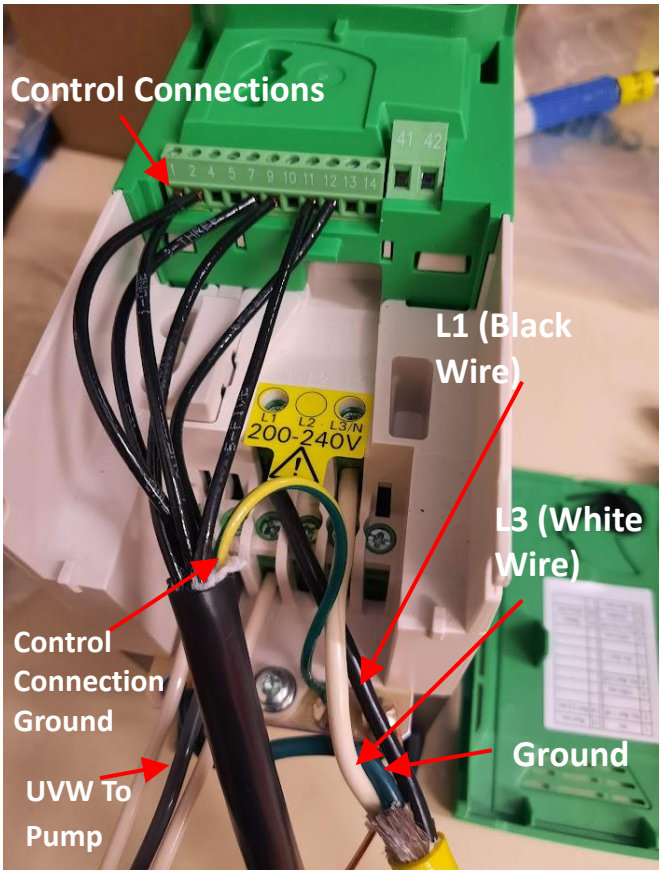

Figure 15. The VFD with connections identified. L1, L3, Ground from the Transformer powers the VFD and pump. UVW To Pump are the connections for the power. The control connections are connected to the Arduino microcontroller.

3.3.3 Arduino Electronics

To attain both controls and data acquisition from a singular source, an Arduino Leonardo is utilized. The wiring diagram (Figure 16) shows the different connections which all convene at the Arduino. Due to the nature of having varying sensors of different models and manufacturers, it is imperative that the Arduino can process all the incoming data. Most of the pins (A0-A5 and some of the digital pins) read analog inputs of 0-5V in linearly, which is sufficient for most sensors such as the pressure transducer and flowmeters. The Leonardo was chosen due to the number of sensors involved, as other Arduino devices do not have enough pins to accommodate all the sensors (Figure 17). All the connections share the same grounding, to ensure safety. To establish a connection between the PC and Arduino, the Arduino IDE is used with the setup wizard.

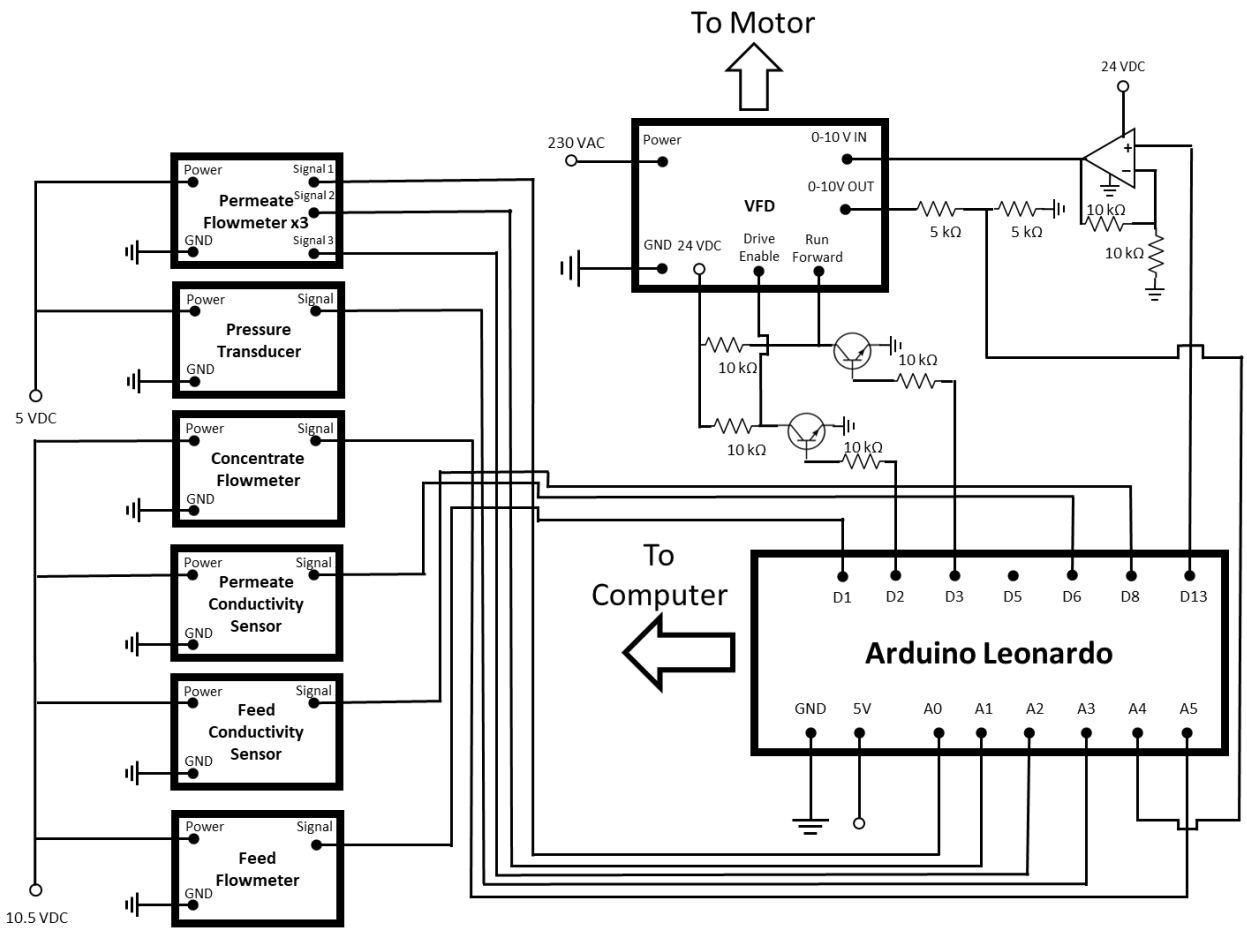

Figure 16. The wiring diagram for the various sensors and controls of the Arduino and VFD.

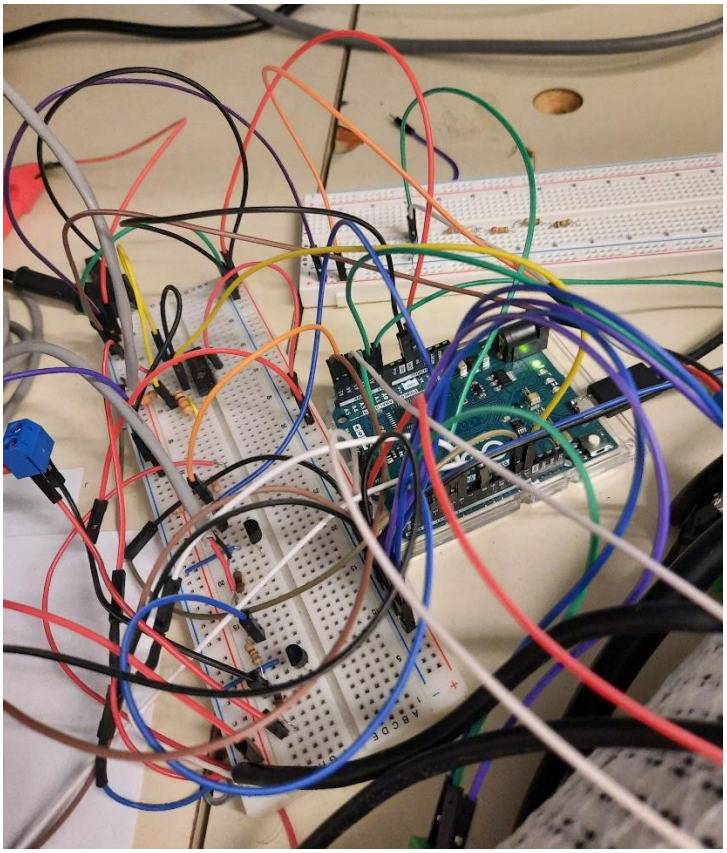

Figure 17. The Arduino Leonardo connected to the various sensors through the breadboard circuit.

3.3.4 LabVIEW UI and Data Collection

All the electrical components mentioned above need a central hub in which to control and view data. The integration of LabVIEW combines the sensor's voltage outputs, calibration curves, the Arduino and VFD controls, and an easy-to-use front-end interface for the user. In this section, the efforts to implement this idea from the back-end is described. The circuitry of all components is also described, as not all controls and sensors operate in the same manner.

Integrating LabVIEW involved firstly connecting the Arduino to LabVIEW itself. Unfortunately, the setup wizard with LINX (a LabVIEW Virtual Instrument (VI) for Arduino and other controllers) did not work as intended. The workaround was to manually flash the

LINX_Arduino_Base_Firmware.ino file onto the Leonardo prior to selecting the COM port. The LabVIEW block diagram shown in Figure 18 displays the backend programming implemented for the system. LINX Open serial VI on the top left establishes the connection with the Arduino on the specified COM port. The program then connects to the specified Analog Read X Chan VI's, that receives 0-5 V signals from the respective sensor. Each signal is converted to the corresponding value (pressure, flowrate, etc.) by calibrated conversions provided by the manufacturer. The values are also displayed on the front panel, shown in Figure 19, as well as graphs to monitor changes over a specified period. All the calculated values are written into a spreadsheet, which can then be analyzed once the experiment has concluded.

The VFD pump controls are seen in Figure 18 (b), by the Digital Write Chan VI's. The Drive Enable and Run Forward switches are used to enable the pump, while the Set Duty Channel VI is used to set the frequency of the drive. The Drive Enable and Run Forward switches utilize a transistor setup that enables/disables the current flow from each pin. The op-amp is used to provide a gain to the VFD, as the duty cycle receives 0-10 V power, but the Arduino is only capable of outputting 0-5 V. There is a safety feature included in case the pressure of the system increases beyond a set value, whereby the duty cycle will be decreased by a set value. This in combination with the pressure relief valve ensures safety of the system while operating.

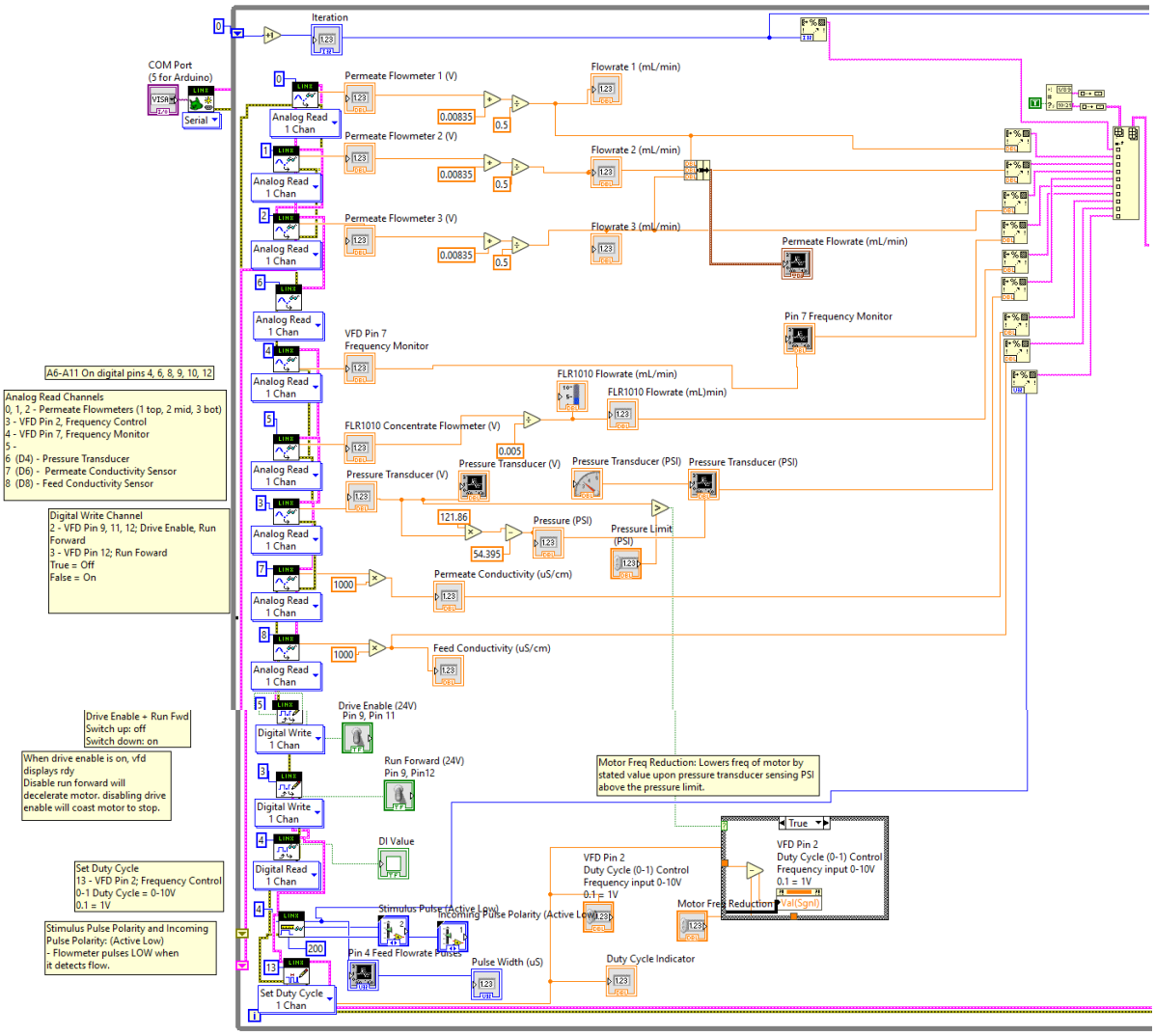

Figure 18. The block diagram for the LabVIEW program.

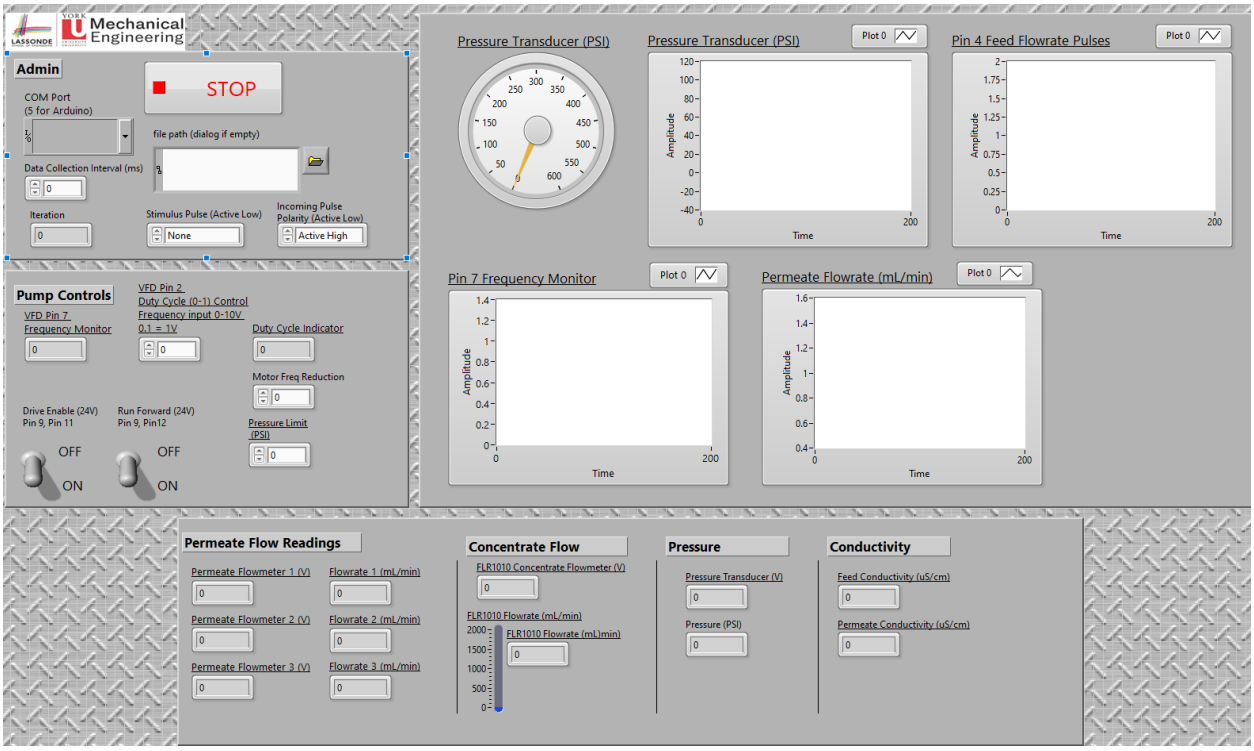

Figure 19. The LabVIEW front panel UI.

3.4 Experimental Methods

In this section, the processes involved to undergo an experiment are described. The framework of how experimentation is executed, what factors are being tested, and how results can be interpreted are detailed. Due to time constraints and longer than anticipated completion date for the experimental system, the methods and results are based off previous experimental research work and reported methods rather than empirical data collected.

3.4.1 Experimental Water Procurement

There are several possibilities for feed water choices that can be sourced locally. Prior to the complex water experimentation, a simple saline solution of 0.05 wt.% NaCl would be run to ensure the system is able to adequately perform RO with the membrane's rated salt rejection. Then,

water from a local well such as in Nobleton, Ontario can be sourced to provide water with a variety of salts and mineral content, in addition to a small amount of organic matter. Table 4 shows the water content of the Nobleton, ON well and an experimental water matrix that was concocted by the addition of salts to the well water. The concentrations added were tailored to mimic the water chemistry of groundwater in La Mancalona, Mexico, where an earlier implementation of a PVRO was conducted [40]. The desired salt content is achieved with lab-grade chemicals of magnesium sulfate, sodium chloride, sodium sulfate, and calcium sulfate. It is desirable that the water chemistry contains few organic and biological contaminants for this particular experiment, as it is uncertain whether coated membrane modules perform well with feed sources more complex than one or two foulants at a time.

Table 4. Water chemistry of well water in Nobleton, Ontario and experimental groundwater-based matrix [40].

Ion in Water	**Nobleton, Ontario Deep Well (mg/L)**	**Experimental Groundwater-based Matrix (mg/L)**	**La Mancalona, Mexico Groundwater (mg/L)**
Sodium (Na^{2+})	11	164	164
Magnesium (Mg^{2+})	26	99	99
Calcium (Ca^{2+})	64	502	502
Chloride (Cl^{-})	2.3	166	166
Sulfate (SO_4^{2+})	-	1436	1773
Potassium	-	-	6.4
Iron	-	-	5.9
Nitrate as Nitrogen	-	-	3.9
Silicon	22	22	23
Strontium	0.75	0.75	12
General Characteristics			
pH	7.63	7	7.83
Alkalinity	1.2		142.5
Conductivity	550	3740	3770
Total Dissolved Solids (TDS)	340	2393	2262
Hardness	270	1660	1661
Dissolved Organic Content (DOC)	2.9	2.9	1.3
Total Ammonia-N	3.7	3.7	0.37

3.4.2 Operating Conditions

The operating conditions for the system are chosen to mimic both continuous and intermittent operation. The continuous filtration process will occur over a longer period of time (24 hour and longer), whereas the intermittent operation will operate on an 8 hour on, 16 hours off

period. Experimentation would not need to extend for more than 2-3 days, due to the small active membrane area of the CF016D modules. To ensure the purity of the permeate, elemental analysis is used to identify the contents of the permeate. Conductivity is measured throughout the experiment and plotted over time to observe changes that may occur in the permeate or feed channels. Temperature of the feed channel remains consistently room temperature and can be measured externally. The pressure of the system is set at around 2758 kPa, using the needle valves (SS-20VS4, Swagelok) at each recirculation line leading from the RO modules. These valves are adjusted over time as fouling occurs, to ensure the pressure remains adequate for permeate flow. Each individual valve is manual and altering the position of one valve changes the pressure for all three lines. To this end, operating the system requires careful adjustments to ensure all three systems are at similar pressure and recirculation flowrate.

3.4.3 Membrane Coupon Preparation

The membranes procured for the experiments are the TM720D, sourced from Toray, USA. These aromatic PA TFC membranes are fabricated for brackish water, offering minimum 99.65% salt rejection. The membrane is cut into a smaller coupon using a die (Sterlitech CF016 Steel Rule Die, 58 x 75 mm). The shape of the coupon is shown in Figure 20, with two holes allowing for alignment into the RO modules' screws. The membranes are submersed in MilliQ® water for 24 hours prior to use to ensure maximum water swelling is achieved prior to experimentation. Prior to experiments, the membrane is pre-compacted into the RO module by operating the system at 2758 kPa for 2 hours using MilliQ water. These two steps ensure uniform polymer swelling and a reliable fit for the full extended experiment duration. To create a tight seal along the shape of the active area, O-rings are used to conform to the shape of the RO module.

3.4.4 Membrane Autopsy and Analysis

Once the experiments have concluded, the individual RO membranes are released from the modules and prepared for SEM. A small portion of the active area is cut from the same location throughout all experiments, shown in Figure 20. Other sections of the membrane may be used for XRD in a similar manner. To ensure consistency throughout results, the cut location for all samples remains the same for the particular characterization method.

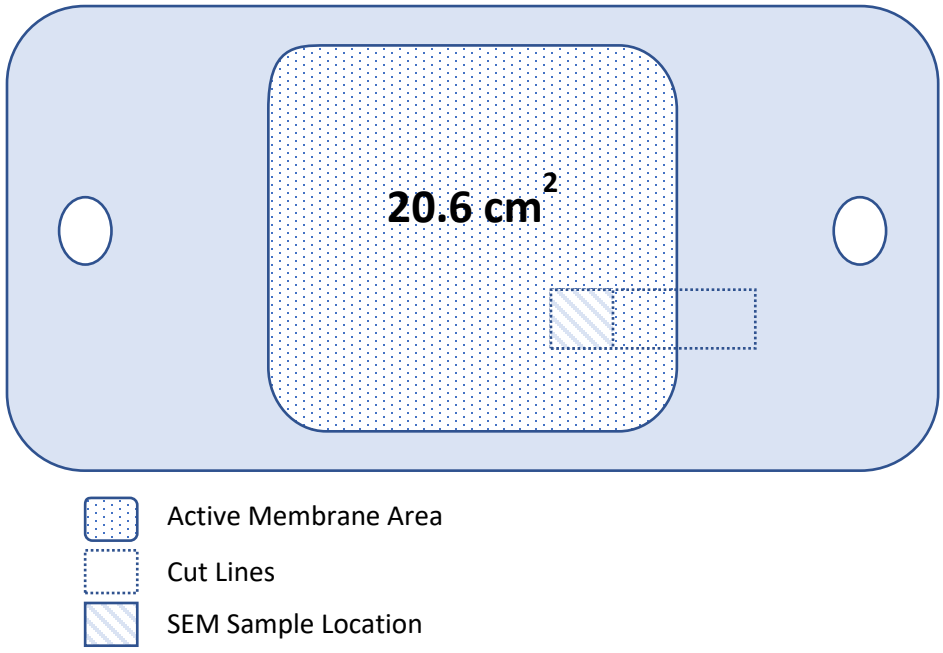

Figure 20. The approximate size and surface area scheme of the membrane coupon for the CF016D.

Other analytical methods to be employed are focused on the structural and chemical properties of the membrane itself, rather than foulants or scalants deposited on top. To analyze the hydrophilicity of the system, water contact angles (WCA) is employed. Surface roughness and

zeta potential are used to assess the topography and surface charge of the membrane respectively. To identify the functional groups on the surface of the membrane coating, FTIR is employed.

3.4.5 Permeate Decline Analysis

One of the primary methods to determine the membrane's performance over time is the permeability. The highest performance possible for a given set of operating conditions comes from the pristine, clean membrane before it has been used, and thus fouled. This maximum permeability, which is recorded within the first hour of operating the system, is used as a benchmark for permeability decline throughout the remainder of the experiment. To calculate the normalized permeability P_n, take the ratio of the initial flowrate Q_{ti} and the flowrate at a later time Q_{t2}, as seen in Equation 1.

Equation 1. $$P_n = \frac{Q_{t2}}{Q_{ti}}$$

As foulants accumulate on the membrane surface over hours and throughout the shutdown periods for intermittently operated RO, the permeability declines substantially, calculated as a fraction of the permeability at the beginning of the experiment. This normalized permeability is plotted over time for each RO module and is used as a proxy for fouling rate. For example, if the normalized permeability drops to half of the original rate over 48 hours for pristine membranes, but only a quarter for a membrane coated with polydopamine, the fouling rate for the coated membrane would be concluded as lesser. This does not consider the absolute permeability, however, which can be analyzed by comparing the flowrates directly at a given point in time. The absolute fouling is also not accounted for here, but rather through SEM results.

Another way to look at permeability decline is the recovery rate. Somewhat analogously, the recovery rate is the percentage of feed water that gets filtered into permeate. It is desirable to maintain a high recovery rate, such that the overall output of the system remains feasible for its main purpose.

3.5 Initial Testing Results

Once the system's construction was completed, initial testing to validate that the RO modules can successfully achieve cross flow reverse osmosis was conducted. To do so, distilled water of minimal salinity was used in this experiment. This section details the results of said experiments, including the data collected. Experiments A and B were obtained on December 12, 2022. The distilled water was obtained through the technical services offered at the Petrie Science & Engineering Building. In the subsequent graphs and data discussed, flowmeters denoted as "1", "2", and "3" refer to the RO modules labelled in Figure 21.

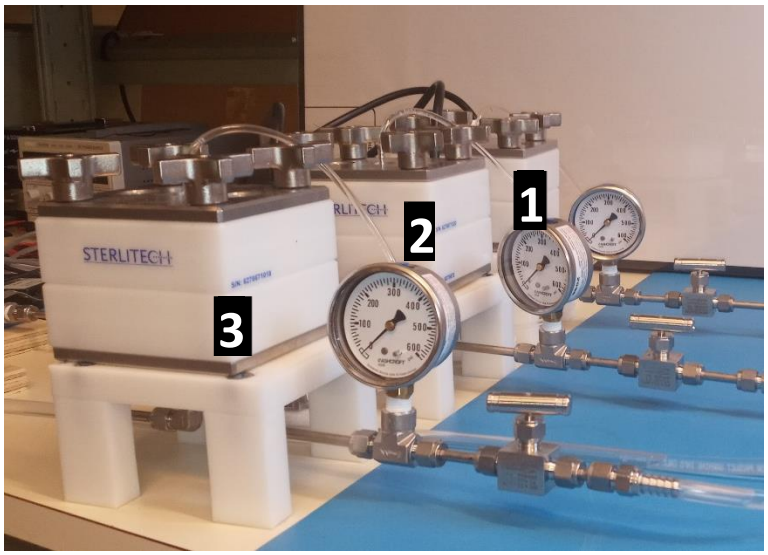

Figure 21. The labelled RO modules used to denote their respective flowmeters.

3.5.1 Experiment A

In Experiment A, a 40-minute course was conducted to illustrate the process of membrane compression which occurs during the initial start-up of the system. During this pre-compaction phase, the permeability is expected to be variable, as the membrane is actively adjusting to the environment that is the RO module. The pressure of the system is also expected to shift because of the membrane compression process.

Figure 22 shows the permeate flowrate over a 42 minute period for RO module 1. Figure 23 shows the same data overlaid with flowmeters 2 and 3. As seen in all three flowmeters, the flowrate from minutes 0-2 are variable as the system starts to turn on. Throughout minutes 2-20, there are significant flucuations in the permeate flowrates for all three flowmeters. Some of these fluctuations are due to changes in pressure, as seen in Figure 24. The pressure was lowered back to 400 psi using the needle valves when the pressure reached upwards of 450 psi. Some fluctuations where the pressure drops to below 300 psi are due to the high sensitivity of the needle valves, whereby opening the valve slightly more than required would drop the pressure significantly.

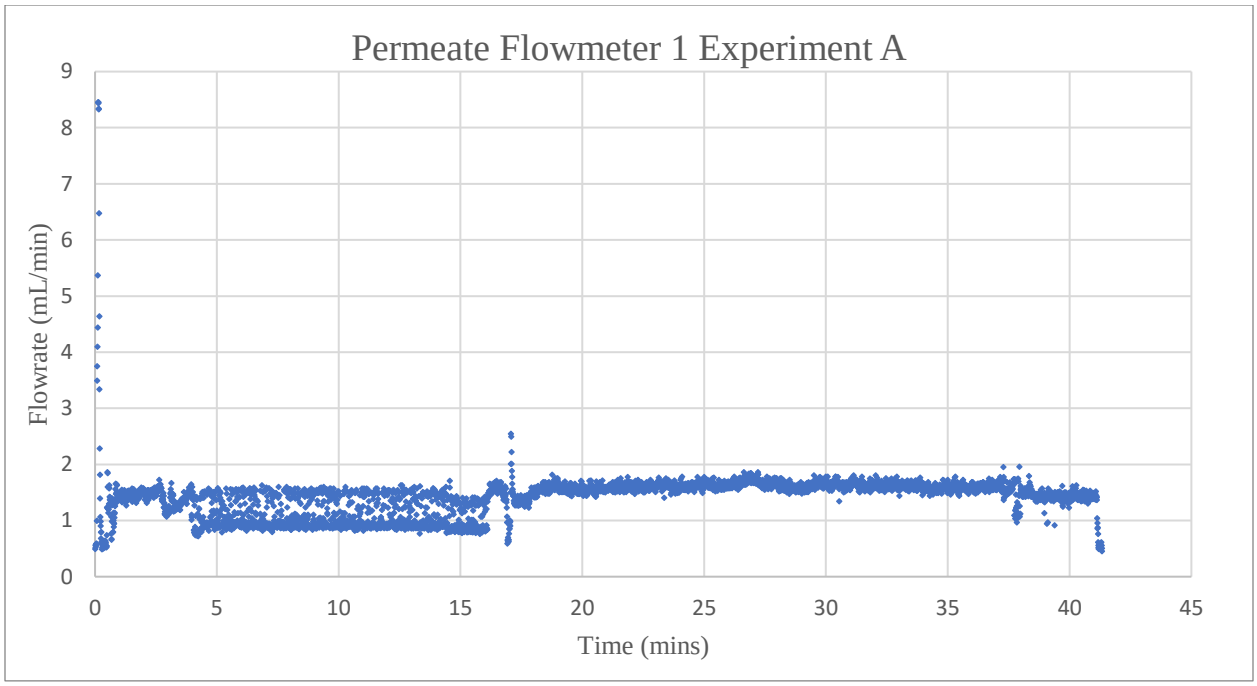

Figure 22. Permeate Flowrate of single RO module pre-compaction.

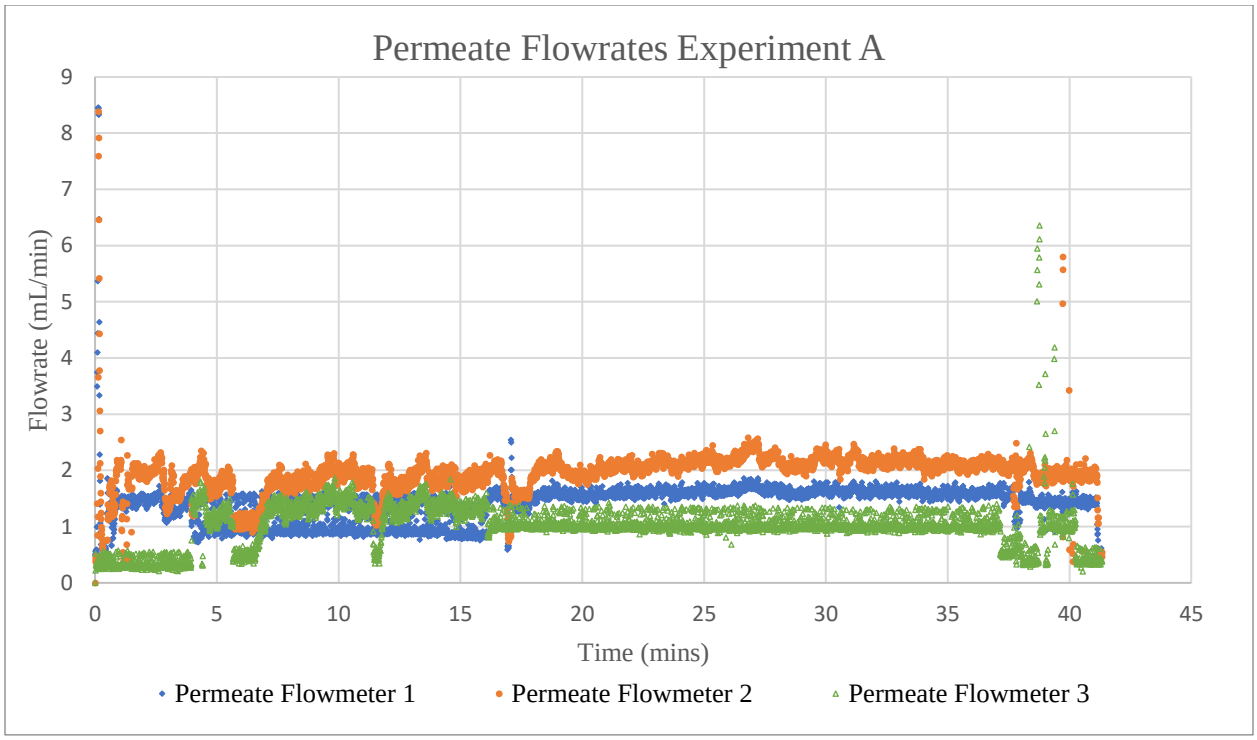

Figure 23. Permeate flowrates for all three flowmeters.

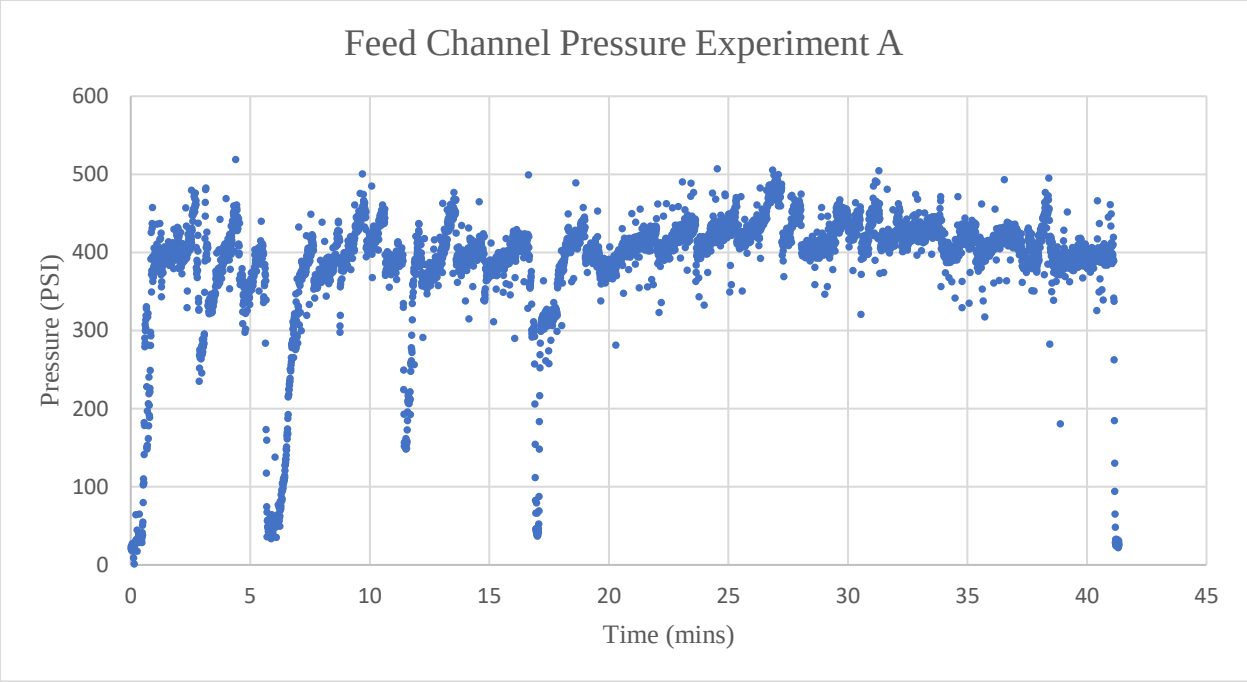

Figure 24. Pressure of feed channel for experiment A.

The pressure and permeate are closely correlated, as dropping the pressure below a certain threshold also lowered the permeate flowrate, as seen in Figure 25. The experiment was concluded at the 41-minute mark, where the pump frequency was brought to 0 Hz and the pressure and flowrate drop to their minimums, as seen by the drop at the end of the data.

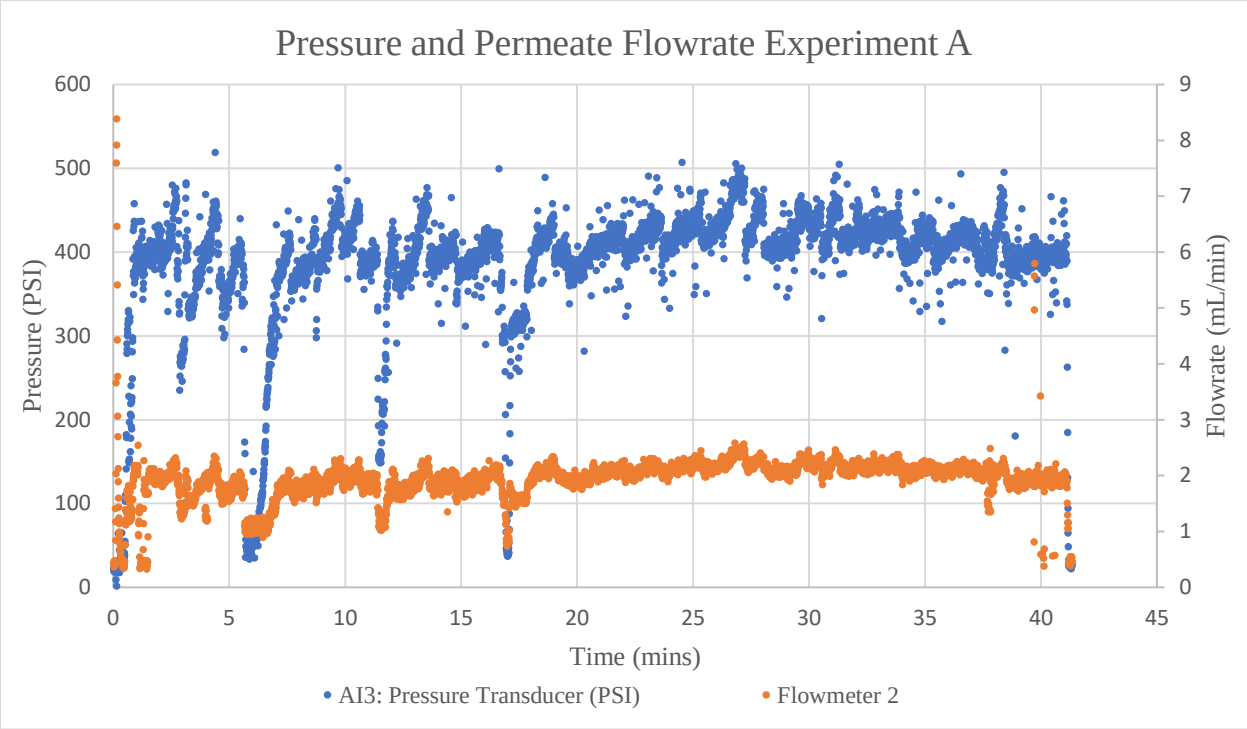

Figure 25. Pressure and flowrate overlaid together to show trends.

The recirculation flowrate shown in Figure 26 shows consistent jumps in the flowrate over time, after the initial phase where the system is in start-up. The increases in flowrate at 3, 12, and 17 minutes are due to the increase in pump frequency from 0.3 to 0.4 to 0.5 duty cycle. This corresponds to approximately 5 Hz, 7 Hz, and 9 Hz on the VFD. The pump frequency increases cause more water to flow through the system, thus increasing the recirculation flowrate. There is a large dip in flowrate at the 17-minute mark due to an operational error whereby the duty cycle was set to 0 for that moment but was noticed and quickly brought back to the original value.

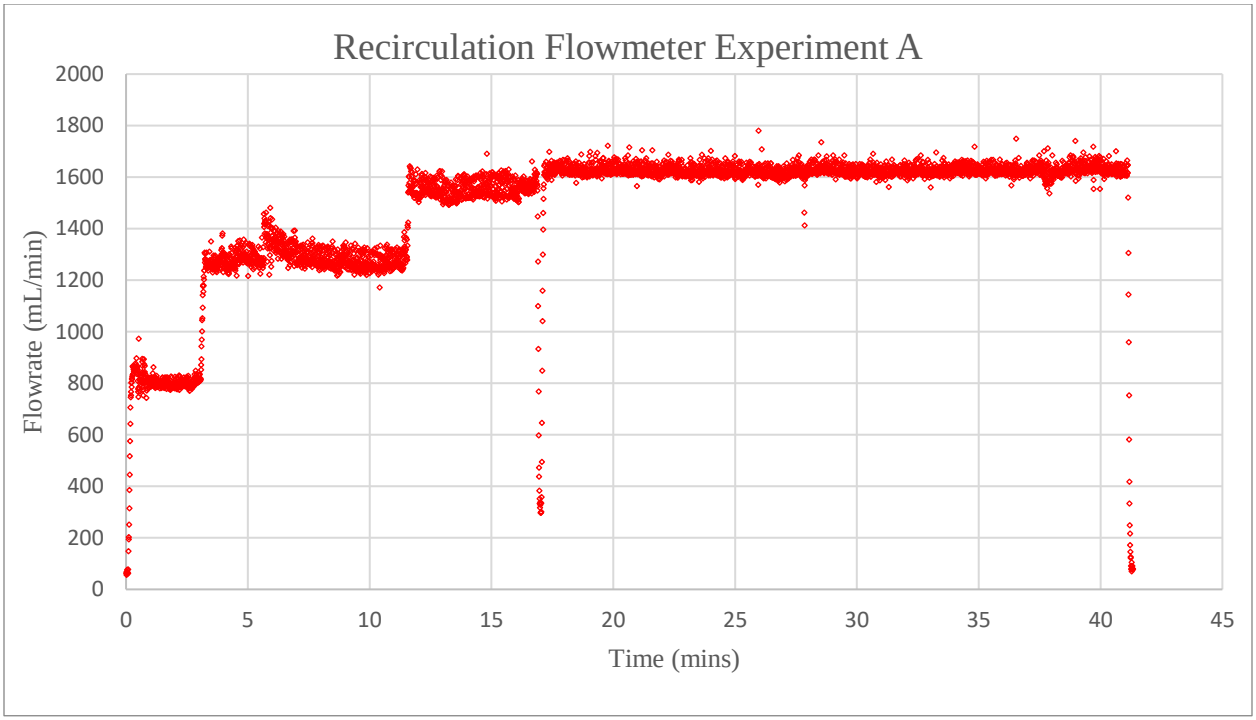

Figure 26. Recirculation flowrate for experiment A.

The conductivity of the feed and permeate channels are expected to be similar since there are no salts added to the system. The salinity of the distilled water is expected to be very low and thus the conductivity should also be lower than high salinity feed waters. Figure 27 shows the conductivity of both the feed and permeate lines. The conductivities are very similar, with minor shift higher for the permeate sensor that may be attributed to calibration differences.

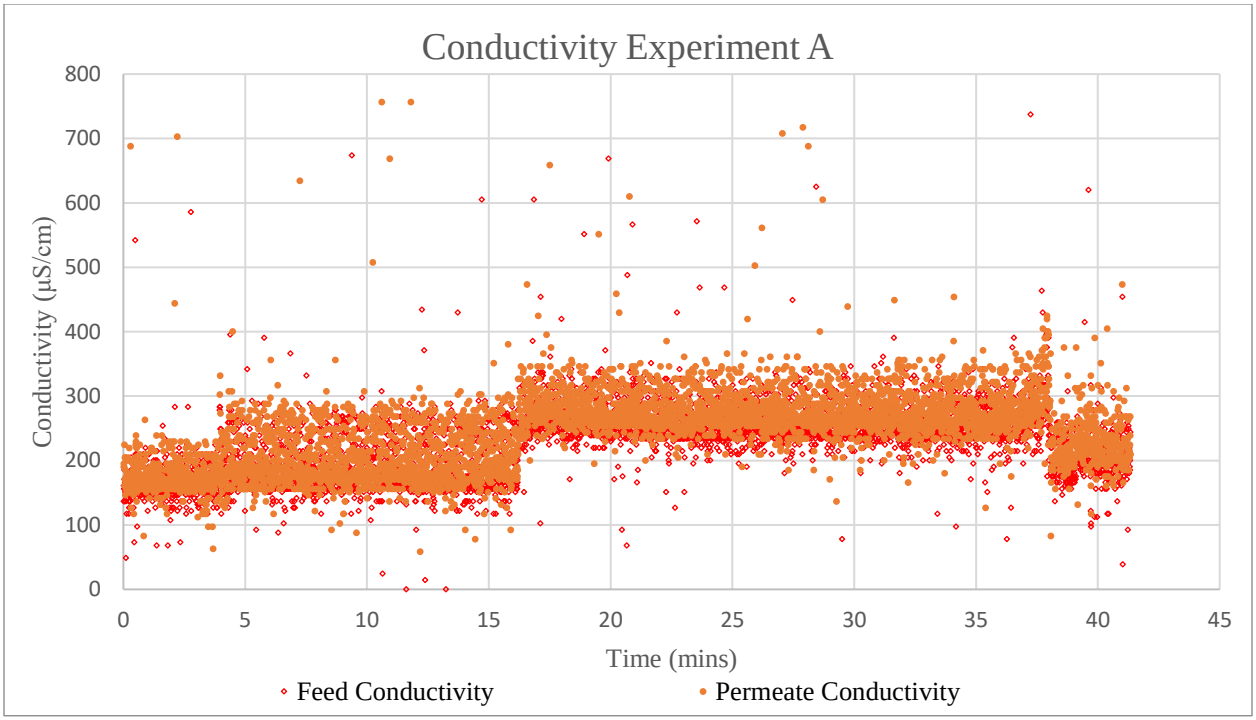

Figure 27. Conductivity of the feed (red) and permeate (orange) channels for experiment A.

3.5.2 Experiment B

Experiment B consists of 65 minutes of cross flow shortly after the conclusion of experiment A. The parameters remain the same, as the pressure was kept at 400 psi and adjusted with the needle valves. Figure 28 shows the three permeate flowrates over the 65-minute period. The flowrates appear to be more stable than in experiment A, as the membrane has completed its compression and is now ready for operation.

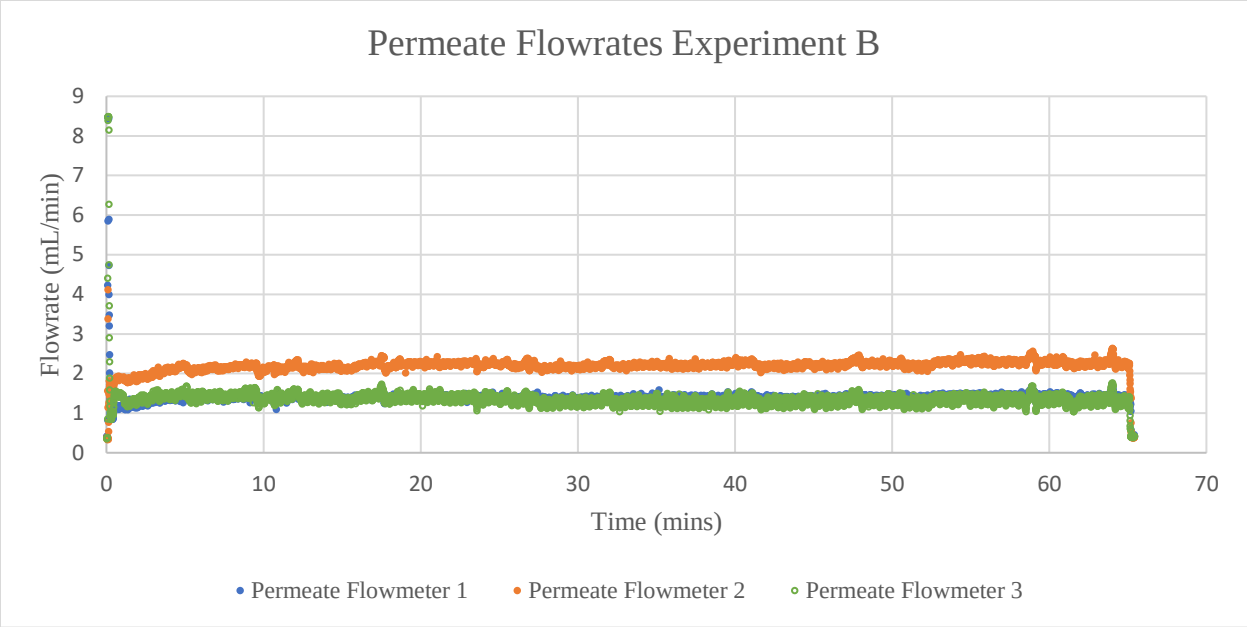

Figure 28. Permeate Flowrates for experiment B.

The pressure in experiment B was more stable than in experiment A. Qualitatively, observing changes to the needle valve positions was substantially less often required during this experiment. This can be seen quantitatively in Figure 29, where there is less fluctuation in the pressure in experiment B (blue) than A (orange). Figure 30 Also shows experiment B pressure and flowrate, where small fluctuations still cause changes in the flowrate, but to a lesser degree than experiment A, in Figure 25.

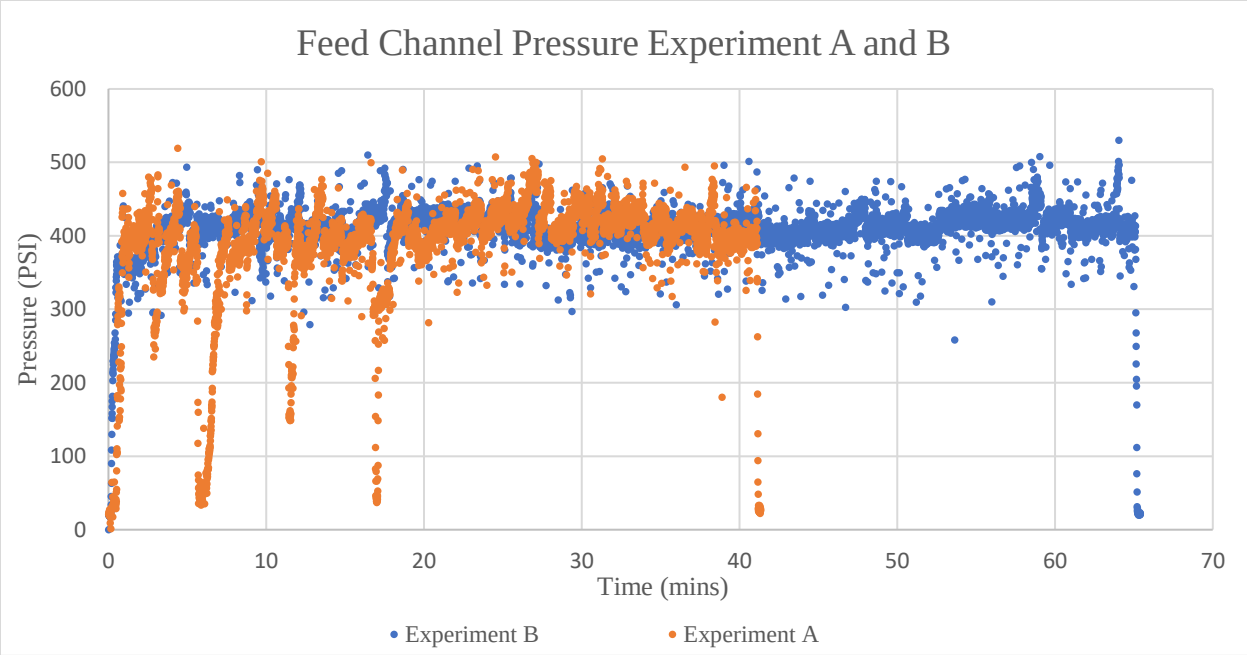

Figure 29. Pressure of Experiments A and B).

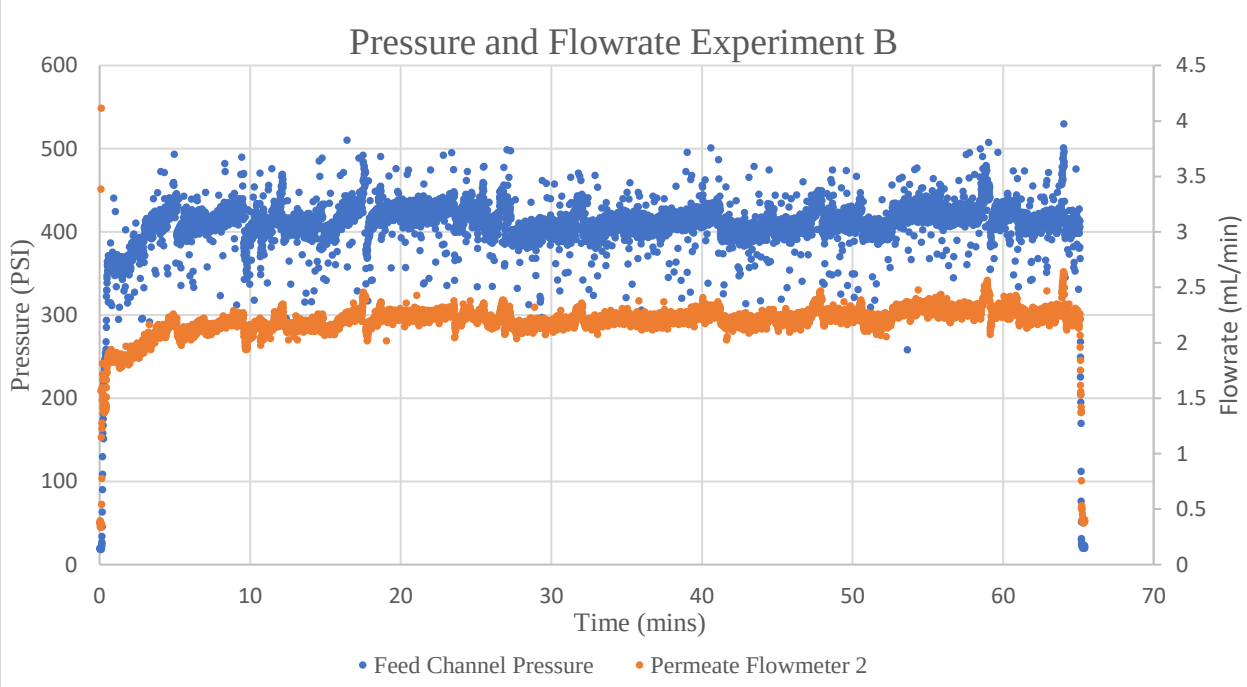

Figure 30. Pressure and flowrate for experiment B.

The recirculation flowmeter is also very consistent, as seen in Figure 31. The frequency of the drive was immediately brought to 0.5 (9.7 – 9.9 Hz), thus there are no large fluctuations in

flowrate throughout the experiment. Figure 32 shows the conductivity once more, with little to no fluctuations as the system has properly initialized after experiment A.

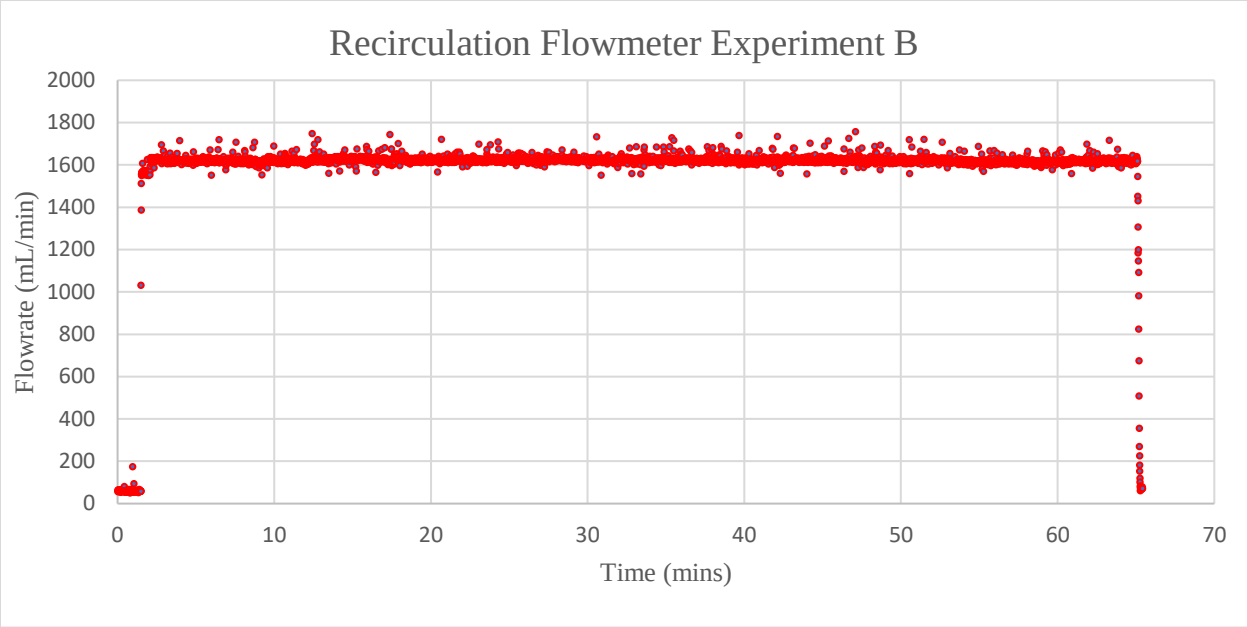

Figure 31. Recirculation flowmeter for experiment B.

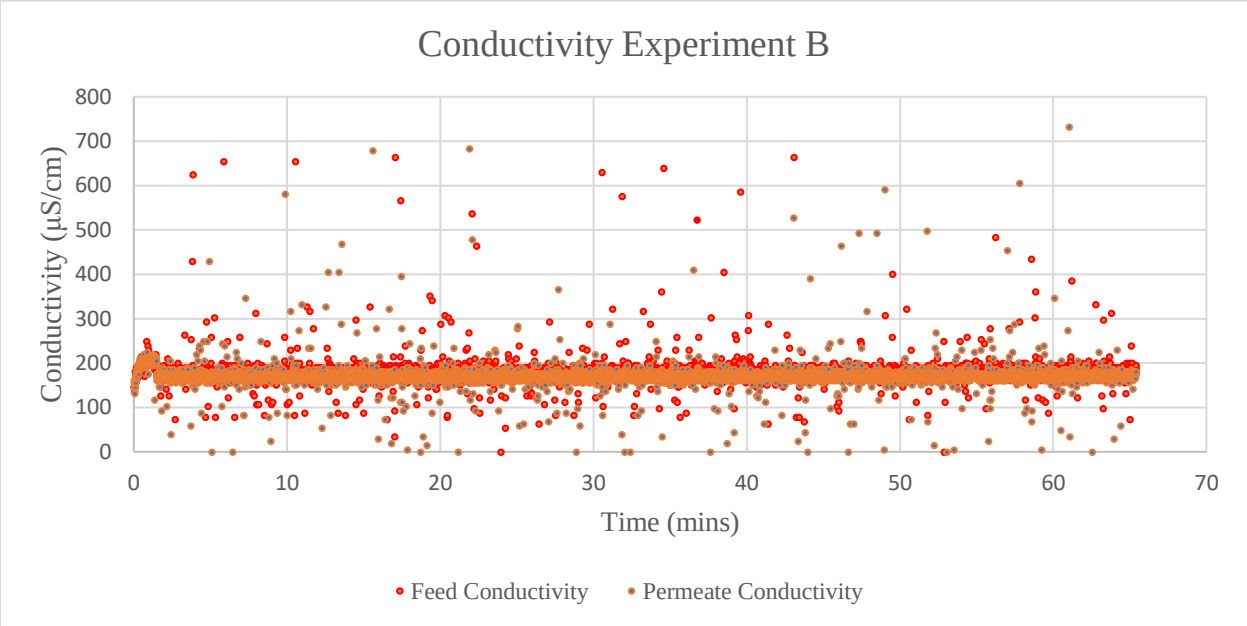

Figure 32 Conductivity of feed (red) and permeate (orange) channels for experiment B.

3.5.3 Discussion

The initial experiment using the distilled water sample was successful. The system is able to operate for long periods of time and collect data without significant setbacks. There were some

minor issues with the connectivity of the flowmeters, which can be resolved by exchanging the current circuitry with a more permanent solution once the system has been tested more. The needle valves used to adjust the pressure of the system was simple and effective, producing immediate changes that can be fine-tuned within ±25 psi.

There are some small differences between the flow rates of the three RO modules. This can be attributed to the structure of the plumbing, as the center module (connected to flowmeter 2) has the shortest and most direct path for water to flow through, compared to modules 1 and 3 (see Figure 11). Thus, the flowrate is slightly higher than modules 1 and 3, which have comparable flowrates. This difference can be worked around by normalizing the permeability. By calculating the permeability decline over time compared to the permeability immediately post-compression, the normalized permeability can be used to quantify membrane fouling and degradation over time.

3.6 Conclusions

The lab-scale RO system created for membrane coating and fouling experiments was constructed and simple to operate. There were significant challenges during the construction, due to a combination of logistical and compatibility issues. Many parts ordered took lengthy amounts of time to be fulfilled, due to supply chain issues. The system's tolerance to high pressures was a key factor in planning the choice of components related to the plumbing. To facilitate higher pressures and low corrosion, all essential components are high-pressure resistant stainless steel.

The integration with Arduino and LabVIEW was also challenging, due to the variety of sensors involved. Some sensors behave differently in terms of voltage output than others, while the required input voltage of each sensor and controller can vary as well. 5V, 12V, 110V, and 220V power are used as inputs for the system. The system is simple to control through LabVIEW

but requires some understanding of how the Arduino firmware is loaded (found in the operations guide separately). It is viable to continue with experimentations relating to coatings and/or intermittent & continuously operated systems.

Chapter 4

4 Summary and Conclusions

4.1 Summary

This thesis presented the framework on membrane fouling, coatings, and intermittent operation in RO systems. The role of RO desalination in delivering potable water for small, rural communities was discussed. The viability of renewable powered PVRO systems was also discussed. Fouling mechanisms that occur by inorganic, organic, and biological contaminants was summarized. Several factors relating to membrane surface properties to mitigate fouling was covered in the context of brackish feed water sources that contain a complex matrix of contaminants. The process of planning, sourcing parts, and constructing a lab-scale RO system was reported. The methodology in which to conduct experiments relating to membrane preparation, analytical methods, operating the system, and interpreting results is discussed. Preliminary testing of the system with distilled water found that there is an approximately 60-minute initialization phase, whereby the membranes are packed into the modules prior to operating the system. During this period, parameters such as flowrates, pressure, and conductivity can vary. Once the system completes the initialization phase, it was found that these parameters stabilized.

4.2 Conclusions

Intermittently operated systems have been reported as viable in scenarios where renewable energy is sufficient to power the system for 8 hours of a day. There is also extensive literature on

the viability of specific membrane coatings to combat fouling of inorganic, organic, and biological varieties. Currently, there are no studies on the behaviour of surface-modified membranes in intermittently operated RO systems. Additionally, complex water matrices such as brackish and seawater RO has not been explored for most membrane coatings. This thesis provides the foundation for future research into these areas of desalination. The modularity of the RO system facilitates experiments of different objectives, and quick turnaround for membrane fouling experiments. The Arduino and LabVIEW interface is fluid and can be configured with more sensors, or other functionality as well. In summary, objective 1 was completed while objectives 2 and 3 were not completed due to the delays stemming from COVID-19 health and safety related shutdowns and supply chain issues.

4.3 Directions for Future Work

There are several directions in which this work may be continued. Interest in membrane coatings for antifouling performance can be investigated due to the small surface area of the membrane coupons, allowing for easy application of the coating at the lab scale. Smaller surface areas also facilitate quicker fouling timelines, allowing for quick turnover. The presence of three RO modules allows for comparison between coated and pristine membranes within the same experiment if there is interest. Analysis of the recovery rate, in addition to permeate decline, would provide insight into the viability of membrane coatings for larger scale systems when it comes to daily permeate output. There is a balance of coating thickness and type to the recovery rate that has not been explored currently. Changes in weather conditions causing feed water quality fluctuations may be explored in the context of membrane coatings and intermittent operation to better reflect real-life weather events.

Renewable energy powered RO can also be studied due to the ease of turning on and off the system. Intermittent RO is an emerging desalination avenue for small-scale communities. Future work into optimizing intermittent operation with rinsing, anti-scaling reagents, feed water type, are all possible. In addition to PVRO, wind or hydropower systems may be integrated into RO systems. An optimization framework for intermittent operation that extends beyond the 8/16 schedule of PV cells may be of interest. The permeate flux and fouling behaviours are also unexplored in this realm. Combining membrane coatings with intermittent RO is a field that is largely unexplored, and thus contains plenty of space for innovation.

References

[1] "Progress on household drinking water, sanitation and hygiene 2000–2020: Five years into the SDGs," Sep. 2021, doi: ISBN 978 92 4 003084 8.

[2] "The United Nations world water development report 2018: nature-based solutions for water - UNESCO Digital Library." https://unesdoc.unesco.org/ark:/48223/pf0000261424 (accessed May 30, 2022).

[3] N. J. Ashbolt, "Microbial contamination of drinking water and disease outcomes in developing regions," *Toxicology*, vol. 198, no. 1, pp. 229–238, May 2004, doi: 10.1016/j.tox.2004.01.030.

[4] H. Morais, P. Kádár, P. Faria, Z. A. Vale, and H. M. Khodr, "Optimal scheduling of a renewable micro-grid in an isolated load area using mixed-integer linear programming," *Renew. Energy*, vol. 35, no. 1, pp. 151–156, Jan. 2010, doi: 10.1016/j.renene.2009.02.031.

[5] A. I. Schäfer, G. Hughes, and B. S. Richards, "Renewable energy powered membrane technology: A leapfrog approach to rural water treatment in developing countries?," *Renew. Sustain. Energy Rev.*, vol. 40, pp. 542–556, Dec. 2014, doi: 10.1016/j.rser.2014.07.164.

[6] B. Peñate and L. García-Rodríguez, "Current trends and future prospects in the design of seawater reverse osmosis desalination technology," *Desalination*, vol. 284, pp. 1–8, Jan. 2012, doi: 10.1016/j.desal.2011.09.010.

[7] I. de la Nuez Pestana, F. Javier García Latorre, C. Argudo Espinoza, and A. Gómez Gotor, "Optimization of RO desalination systems powered by renewable energies. Part I: Wind energy," *Desalination*, vol. 160, no. 3, pp. 293–299, Jan. 2004, doi: 10.1016/S0011-9164(04)90031-8.

[8] A. M. Delgado-Torres and L. García-Rodríguez, “Status of solar thermal-driven reverse osmosis desalination,” *Desalination*, vol. 216, no. 1–3, pp. 242–251, Oct. 2007, doi: 10.1016/j.desal.2006.12.014.

[9] E. Antipova, D. Boer, L. F. Cabeza, G. Guillén-Gosálbez, and L. Jiménez, “Uncovering relationships between environmental metrics in the multi-objective optimization of energy systems: A case study of a thermal solar Rankine reverse osmosis desalination plant,” *Energy*, vol. 51, pp. 50–60, Mar. 2013, doi: 10.1016/j.energy.2013.01.001.

[10] R. Salcedo, E. Antipova, D. Boer, L. Jiménez, and G. Guillén-Gosálbez, “Multi-objective optimization of solar Rankine cycles coupled with reverse osmosis desalination considering economic and life cycle environmental concerns,” *Desalination*, vol. 286, pp. 358–371, Feb. 2012, doi: 10.1016/j.desal.2011.11.050.

[11] A. M. Bilton, “A Modular Design Architecture for Application to Community- Scale Photovoltaic-Powered Reverse Osmosis Systems.”

[12] L. Kelley, H. Elasaad, and S. Dubowsky, “Autonomous operation and maintenance of small-scale PVRO systems for remote communities,” *Desalination Water Treat.*, vol. 55, no. 10, pp. 2843–2855, Sep. 2015, doi: 10.1080/19443994.2014.940650.

[13] H. Elasaad, A. Bilton, L. Kelley, O. Duayhe, and S. Dubowsky, “Field evaluation of a community scale solar powered water purification technology: A case study of a remote Mexican community application,” *Desalination*, vol. 375, no. Complete, pp. 71–80, 2015, doi: 10.1016/j.desal.2015.08.001.

[14] W. He, Y. Wang, and M. H. Shaheed, “Stand-alone seawater RO (reverse osmosis) desalination powered by PV (photovoltaic) and PRO (pressure retarded osmosis),” *Energy*, vol. 86, pp. 423–435, Jun. 2015, doi: 10.1016/j.energy.2015.04.046.

[15] S. M. Shalaby *et al.*, “Reverse osmosis desalination systems powered by solar energy: Preheating techniques and brine disposal challenges – A detailed review,” *Energy Convers. Manag.*, vol. 251, p. 114971, Jan. 2022, doi: 10.1016/j.enconman.2021.114971.

[16] “UNICEF Guidance Note: Programmatic approaches to water scarcity,” *UNICEF*, Mar. 2021, Accessed: May 24, 2022. [Online]. Available: https://www.unicef.org/documents/programmatic-approaches-water-scarcity

[17] H. Mahmoudi, N. Ghaffour, M. Goosen, and J. Bundschuh, *Renewable Energy Technologies for Water Desalination*. London: CRC Press, 2017. doi: 10.1201/9781315643915.

[18] F. E. Ahmed, R. Hashaikeh, and N. Hilal, “Hybrid technologies: The future of energy efficient desalination – A review,” *Desalination*, vol. 495, no. Complete, 2020, doi: 10.1016/j.desal.2020.114659.

[19] N. Dhakal, S. G. Salinas Rodriguez, J. C. Schippers, and M. D. Kennedy, “Perspectives and challenges for desalination in developing countries,” *IDA J. Desalination Water Reuse*, vol. 6, no. 1, pp. 10–14, Apr. 2014, doi: 10.1179/2051645214Y.0000000015.

[20] “Total Dissolved Solids (TDS),” p. 3, 1978.

[21] K. P. Lee, T. C. Arnot, and D. Mattia, “A review of reverse osmosis membrane materials for desalination—Development to date and future potential,” *J. Membr. Sci.*, vol. 370, no. 1–2, pp. 1–22, 2011, doi: 10.1016/j.memsci.2010.12.036.

[22] M. Elimelech and W. A. Phillip, “The Future of Seawater Desalination: Energy, Technology, and the Environment,” *Science*, vol. 333, no. 6043, pp. 712–717, 2011.

[23] S. Dallas, N. Sumiyoshi, J. Kirk, K. Mathew, and N. Wilmot, “Efficiency analysis of the Solarflow – An innovative solar-powered desalination unit for treating brackish water,” *Renew. Energy*, vol. 34, no. 2, pp. 397–400, Feb. 2009, doi: 10.1016/j.renene.2008.05.016.

[24] A. M. Gilau and M. J. Small, “Designing cost-effective seawater reverse osmosis system under optimal energy options,” *Renew. Energy*, vol. 33, no. 4, pp. 617–630, Apr. 2008, doi: 10.1016/j.renene.2007.03.019.

[25] A. Cipollina, “Renewable energy desalination: performance analysis and operating data of existing RES desalination plants,” *Desalination Water Treat.*, p. 21, 2015.

[26] T. Younos and C. A. Grady, Eds., *Potable Water: Emerging Global Problems and Solutions*, vol. 30. Cham: Springer International Publishing, 2014. doi: 10.1007/978-3-319-06563-2.

[27] A. W. W. Association and J. Edzwald, *Water Quality & Treatment: A Handbook on Drinking Water, Sixth Edition*. McGraw-Hill Education, 2011. [Online]. Available: http://www.accessengineeringlibrary.com/content/book/9780071630115

[28] D. M. Warsinger, E. W. Tow, K. G. Nayar, L. A. Maswadeh, and J. H. Lienhard V, “Energy efficiency of batch and semi-batch (CCRO) reverse osmosis desalination,” *Water Res.*, vol. 106, pp. 272–282, Dec. 2016, doi: 10.1016/j.watres.2016.09.029.

[29] L. K. Wang, J. P. Chen, Y.-T. Hung, and N. K. Shammas, Eds., *Membrane and Desalination Technologies*. Totowa, NJ: Humana Press, 2011. doi: 10.1007/978-1-59745-278-6.

[30] J. Eke, A. Yusuf, A. Giwa, and A. Sodiq, “The global status of desalination: An assessment of current desalination technologies, plants and capacity,” *Desalination*, vol. 495, p. 114633, Dec. 2020, doi: 10.1016/j.desal.2020.114633.

[31] C. Fritzmann, J. Löwenberg, T. Wintgens, and T. Melin, “State-of-the-art of reverse osmosis desalination,” *Desalination*, vol. 216, no. 1–3, pp. 1–76, Oct. 2007, doi: 10.1016/j.desal.2006.12.009.

[32] G. L. Meerganz von Medeazza, “‘Direct’ and socially-induced environmental impacts of desalination,” *Desalination*, vol. 185, no. 1–3, pp. 57–70, Nov. 2005, doi: 10.1016/j.desal.2005.03.071.

[33] A. Bermudez-Contreras, M. Thomson, and D. G. Infield, “Renewable energy powered desalination in Baja California Sur, Mexico,” *Desalination*, vol. 220, no. 1–3, pp. 431–440, Mar. 2008, doi: 10.1016/j.desal.2007.01.046.

[34] A. Alkhatib, “Reverse-Osmosis Desalination of Water Powered by Photo-Voltaic Modules,” *Comput. Water Energy Environ. Eng.*, vol. 3, no. 1, Art. no. 1, Dec. 2013, doi: 10.4236/cweee.2014.31003.

[35] B. Peñate, V. J. Subiela, F. Vega, F. Castellano, F. J. Domínguez, and V. Millán, “Uninterrupted eight-year operation of the autonomous solar photovoltaic reverse osmosis system in Ksar Ghilène (Tunisia),” *Desalination Water Treat.*, pp. 1–8, Dec. 2014, doi: 10.1080/19443994.2014.940643.

[36] A. Al-Karaghouli, D. Renne, and L. L. Kazmerski, “Technical and economic assessment of photovoltaic-driven desalination systems,” *Renew. Energy*, vol. 35, no. 2, pp. 323–328, Feb. 2010, doi: 10.1016/j.renene.2009.05.018.

[37] B. G. Keeferi, R. D. Hembree, and F. C. Schrack, “Power With Reverse Osmosis,” p. 15.

[38] M. Elshafei, A. K. Sheikh, and N. Ahmad, “Directly Driven RO System by PV Solar Panel Arrays,” *Open J. Appl. Sci.*, vol. 3, no. 2, Art. no. 2, Jun. 2013, doi: 10.4236/ojapps.2013.32B007.

[39] M. Freire-Gormaly and A. M. Bilton, “Experimental quantification of the effect of intermittent operation on membrane performance of solar powered reverse osmosis desalination systems,” *Desalination*, vol. 435, pp. 188–197, Jun. 2018, doi: 10.1016/j.desal.2017.09.013.

[40] M. Freire-Gormaly and A. M. Bilton, “Impact of intermittent operation on reverse osmosis membrane fouling for brackish groundwater desalination systems,” *J. Membr. Sci.*, vol. 583, pp. 220–230, Aug. 2019, doi: 10.1016/j.memsci.2019.04.010.

[41] M. Freire-Gormaly and A. M. Bilton, “Design of photovoltaic powered reverse osmosis desalination systems considering membrane fouling caused by intermittent operation,” *Renew. Energy*, vol. 135, pp. 108–121, May 2019, doi: 10.1016/j.renene.2018.11.065.

[42] M. Freire-Gormaly and A. Bilton, “An experimental system for characterization of membrane fouling of solar photovoltaic reverse osmosis systems under intermittent operation,” *DESALINATION WATER Treat.*, vol. 73, pp. 54–63, 2017, doi: 10.5004/dwt.2017.20391.

[43] G.-D. Kang, C.-J. Gao, W.-D. Chen, X.-M. Jie, Y.-M. Cao, and Q. Yuan, “Study on hypochlorite degradation of aromatic polyamide reverse osmosis membrane,” *J. Membr. Sci.*, vol. 300, no. 1–2, pp. 165–171, Aug. 2007, doi: 10.1016/j.memsci.2007.05.025.

[44] J. S. Baker and L. Y. Dudley, “Biofouling in membrane systems — A review,” *Desalination*, vol. 118, no. 1, pp. 81–89, Sep. 1998, doi: 10.1016/S0011-9164(98)00091-5.

[45] S. Jiang, Y. Li, and B. P. Ladewig, “A review of reverse osmosis membrane fouling and control strategies,” *Sci. Total Environ.*, vol. 595, pp. 567–583, Oct. 2017, doi: 10.1016/j.scitotenv.2017.03.235.

[46] S. S. Bucs, N. Farhat, J. C. Kruithof, C. Picioreanu, M. C. M. van Loosdrecht, and J. S. Vrouwenvelder, “Review on strategies for biofouling mitigation in spiral wound membrane systems,” *Desalination*, vol. 434, pp. 189–197, May 2018, doi: 10.1016/j.desal.2018.01.023.

[47] H. Maddah and A. Chogle, “Biofouling in reverse osmosis: phenomena, monitoring, controlling and remediation,” *Appl. Water Sci.*, vol. 7, no. 6, pp. 2637–2651, Oct. 2017, doi: 10.1007/s13201-016-0493-1.

[48] K.-G. Lu and H. Huang, “Dependence of initial silica scaling on the surface physicochemical properties of reverse osmosis membranes during bench-scale brackish water desalination,” *Water Res.*, vol. 150, pp. 358–367, Mar. 2019, doi: 10.1016/j.watres.2018.11.073.

[49] A. Matin, F. Rahman, H. Z. Shafi, and S. M. Zubair, “Scaling of reverse osmosis membranes used in water desalination: Phenomena, impact, and control; future directions,” *Desalination*, vol. 455, pp. 135–157, Apr. 2019, doi: 10.1016/j.desal.2018.12.009.

[50] L. F. Greenlee, D. F. Lawler, B. D. Freeman, B. Marrot, and P. Moulin, “Reverse osmosis desalination: Water sources, technology, and today’s challenges,” *Water Res.*, vol. 43, no. 9, pp. 2317–2348, May 2009, doi: 10.1016/j.watres.2009.03.010.

[51] B. A. Qureshi, S. M. Zubair, A. K. Sheikh, A. Bhujle, and S. Dubowsky, “Design and performance evaluation of reverse osmosis desalination systems: An emphasis on fouling modeling,” *Appl. Therm. Eng.*, vol. 60, no. 1, pp. 208–217, Oct. 2013, doi: 10.1016/j.applthermaleng.2013.06.058.

[52] F. A. Abd El Aleem, K. A. Al-Sugair, and M. I. Alahmad, “Biofouling problems in membrane processes for water desalination and reuse in Saudi Arabia,” *Int. Biodeterior. Biodegrad.*, vol. 41, no. 1, pp. 19–23, Jan. 1998, doi: 10.1016/S0964-8305(98)80004-8.

[53] A. Cunningham, J. Lennox, and R. Ross, *Biofilms: The Hypertextbook*. Montana State University Center for Biofilm Engineering, 2011. Accessed: Jul. 04, 2022. [Online]. Available: https://www.cs.montana.edu/webworks/projects/stevesbook/index.html

[54] H.-C. Flemming, "Reverse osmosis membrane biofouling," *Exp. Therm. Fluid Sci.*, vol. 14, no. 4, pp. 382–391, May 1997, doi: 10.1016/S0894-1777(96)00140-9.

[55] A. Matin, Z. Khan, S. M. J. Zaidi, and M. C. Boyce, "Biofouling in reverse osmosis membranes for seawater desalination: Phenomena and prevention," *Desalination*, vol. 281, pp. 1–16, Oct. 2011, doi: 10.1016/j.desal.2011.06.063.

[56] M. Herzberg and M. Elimelech, "Biofouling of reverse osmosis membranes: Role of biofilm-enhanced osmotic pressure," *J. Membr. Sci.*, vol. 295, no. 1, pp. 11–20, May 2007, doi: 10.1016/j.memsci.2007.02.024.

[57] T. H. Chong, F. S. Wong, and A. G. Fane, "The effect of imposed flux on biofouling in reverse osmosis: Role of concentration polarisation and biofilm enhanced osmotic pressure phenomena," *J. Membr. Sci.*, vol. 325, no. 2, pp. 840–850, Dec. 2008, doi: 10.1016/j.memsci.2008.09.011.

[58] M. Herzberg, S. Kang, and M. Elimelech, "Role of Extracellular Polymeric Substances (EPS) in Biofouling of Reverse Osmosis Membranes," *Environ. Sci. Technol.*, vol. 43, no. 12, pp. 4393–4398, Jun. 2009, doi: 10.1021/es900087j.

[59] L. Song and M. Elimelech, "Theory of concentration polarization in crossflow filtration," *J. Chem. Soc. Faraday Trans.*, vol. 91, no. 19, p. 3389, 1995, doi: 10.1039/ft9959103389.

[60] S. Zhao *et al.*, "Engineering antifouling reverse osmosis membranes: A review," *Desalination*, vol. 499, p. 114857, Feb. 2021, doi: 10.1016/j.desal.2020.114857.

[61] D. J. Miller, D. R. Dreyer, C. W. Bielawski, D. R. Paul, and B. D. Freeman, “Surface Modification of Water Purification Membranes,” *Angew. Chem. Int. Ed.*, vol. 56, no. 17, pp. 4662–4711, 2017, doi: 10.1002/anie.201601509.

[62] G. Kang, M. Liu, B. Lin, Y. Cao, and Q. Yuan, “A novel method of surface modification on thin-film composite reverse osmosis membrane by grafting poly(ethylene glycol),” *Polymer*, vol. 48, no. 5, pp. 1165–1170, Feb. 2007, doi: 10.1016/j.polymer.2006.12.046.

[63] M. Chapman Wilbert, J. Pellegrino, and A. Zydney, “Bench-scale testing of surfactant-modified reverse osmosis/nanofiltration membranes,” *Desalination*, vol. 115, no. 1, pp. 15–32, Mar. 1998, doi: 10.1016/S0011-9164(98)00022-8.

[64] X. Wei, Z. Wang, Z. Zhang, J. Wang, and S. Wang, “Surface modification of commercial aromatic polyamide reverse osmosis membranes by graft polymerization of 3-allyl-5,5-dimethylhydantoin,” *J. Membr. Sci.*, vol. 351, no. 1, pp. 222–233, Apr. 2010, doi: 10.1016/j.memsci.2010.01.054.

[65] Y. Li, S. Huang, S. Zhou, A. G. Fane, Y. Zhang, and S. Zhao, “Enhancing water permeability and fouling resistance of polyvinylidene fluoride membranes with carboxylated nanodiamonds,” *J. Membr. Sci.*, vol. 556, pp. 154–163, Jun. 2018, doi: 10.1016/j.memsci.2018.04.004.

[66] Y. Hu *et al.*, “Enhancing the performance of aromatic polyamide reverse osmosis membrane by surface modification via covalent attachment of polyvinyl alcohol (PVA),” *J. Membr. Sci.*, vol. 501, pp. 209–219, Mar. 2016, doi: 10.1016/j.memsci.2015.12.003.

[67] S. Zhao *et al.*, “Antifouling and antibacterial behavior of polyethersulfone membrane incorporating polyaniline@silver nanocomposites,” *Environ. Sci. Water Res. Technol.*, vol. 3, no. 4, pp. 710–719, Jun. 2017, doi: 10.1039/C6EW00332J.

[68] M. Ben-Sasson, K. R. Zodrow, Q. Genggeng, Y. Kang, E. P. Giannelis, and M. Elimelech, "Surface Functionalization of Thin-Film Composite Membranes with Copper Nanoparticles for Antimicrobial Surface Properties," *Environ. Sci. Technol.*, vol. 48, no. 1, pp. 384–393, Jan. 2014, doi: 10.1021/es404232s.

[69] X. Huang, K. L. Marsh, B. T. McVerry, E. M. V. Hoek, and R. B. Kaner, "Low-Fouling Antibacterial Reverse Osmosis Membranes via Surface Grafting of Graphene Oxide," *ACS Appl. Mater. Interfaces*, vol. 8, no. 23, pp. 14334–14338, Jun. 2016, doi: 10.1021/acsami.6b05293.

[70] M. He *et al.*, "Zwitterionic materials for antifouling membrane surface construction," *Acta Biomater.*, vol. 40, pp. 142–152, Aug. 2016, doi: 10.1016/j.actbio.2016.03.038.

[71] Z. Liao *et al.*, "Incorporating organic nanospheres into the polyamide layer to prepare thin film composite membrane with enhanced biocidal activity and chlorine resistance," *Sep. Purif. Technol.*, vol. 207, pp. 222–230, Dec. 2018, doi: 10.1016/j.seppur.2018.06.057.

[72] S. F. Seyedpour, A. Rahimpour, and G. Najafpour, "Facile in-situ assembly of silver-based MOFs to surface functionalization of TFC membrane: A novel approach toward long-lasting biofouling mitigation," *J. Membr. Sci.*, vol. 573, pp. 257–269, Mar. 2019, doi: 10.1016/j.memsci.2018.12.016.

[73] B. Gottenbos, "Antimicrobial effects of positively charged surfaces on adhering Gram-positive and Gram-negative bacteria," *J. Antimicrob. Chemother.*, vol. 48, no. 1, pp. 7–13, Jul. 2001, doi: 10.1093/jac/48.1.7.

[74] "Influence of membrane surface properties on initial rate of colloidal fouling of reverse osmosis and nanofiltration membranes," *J. Membr. Sci.*, vol. 188, no. 1, pp. 115–128, Jun. 2001, doi: 10.1016/S0376-7388(01)00376-3.

[75] “A new method for modeling rough membrane surface and calculation of interfacial interactions,” *Bioresour. Technol.*, vol. 200, pp. 451–457, Jan. 2016, doi: 10.1016/j.biortech.2015.10.055.

[76] S. H. Maruf, D. U. Ahn, A. R. Greenberg, and Y. Ding, “Glass transition behaviors of interfacially polymerized polyamide barrier layers on thin film composite membranes via nano-thermal analysis,” *Polymer*, vol. 52, no. 12, pp. 2643–2649, May 2011, doi: 10.1016/j.polymer.2011.04.022.

[77] G.-R. Xu, J.-M. Xu, H.-J. Feng, H.-L. Zhao, and S.-B. Wu, “Tailoring structures and performance of polyamide thin film composite (PA-TFC) desalination membranes via sublayers adjustment-a review,” *Desalination*, vol. 417, pp. 19–35, Sep. 2017, doi: 10.1016/j.desal.2017.05.011.

[78] M. Ben-Sasson *et al.*, “In situ formation of silver nanoparticles on thin-film composite reverse osmosis membranes for biofouling mitigation,” *Water Res.*, vol. 62, pp. 260–270, Oct. 2014, doi: 10.1016/j.watres.2014.05.049.

[79] M. Ben-Sasson, X. Lu, S. Nejati, H. Jaramillo, and M. Elimelech, “In situ surface functionalization of reverse osmosis membranes with biocidal copper nanoparticles,” *Desalination*, vol. 388, pp. 1–8, Jun. 2016, doi: 10.1016/j.desal.2016.03.005.

[80] J. R. Ray, W. Wong, and Y.-S. Jun, “Antiscaling efficacy of $CaCO_3$ and $CaSO_4$ on polyethylene glycol (PEG)-modified reverse osmosis membranes in the presence of humic acid: interplay of membrane surface properties and water chemistry,” *Phys. Chem. Chem. Phys.*, vol. 19, no. 7, pp. 5647–5657, 2017, doi: 10.1039/C6CP08569E.

[81] E. Ostuni, R. G. Chapman, R. E. Holmlin, S. Takayama, and G. M. Whitesides, "A Survey of Structure−Property Relationships of Surfaces that Resist the Adsorption of Protein," *Langmuir*, vol. 17, no. 18, pp. 5605–5620, Sep. 2001, doi: 10.1021/la010384m.

[82] S. Chen, J. Zheng, L. Li, and S. Jiang, "Strong Resistance of Phosphorylcholine Self-Assembled Monolayers to Protein Adsorption: Insights into Nonfouling Properties of Zwitterionic Materials," *J. Am. Chem. Soc.*, vol. 127, no. 41, pp. 14473–14478, Oct. 2005, doi: 10.1021/ja054169u.

[83] Z. Yang, Y. Wu, J. Wang, B. Cao, and C. Y. Tang, "*In Situ* Reduction of Silver by Polydopamine: A Novel Antimicrobial Modification of a Thin-Film Composite Polyamide Membrane," *Environ. Sci. Technol.*, vol. 50, no. 17, pp. 9543–9550, Sep. 2016, doi: 10.1021/acs.est.6b01867.

[84] H. Karkhanechi, F. Razi, I. Sawada, R. Takagi, Y. Ohmukai, and H. Matsuyama, "Improvement of antibiofouling performance of a reverse osmosis membrane through biocide release and adhesion resistance," *Sep. Purif. Technol.*, vol. 105, pp. 106–113, Feb. 2013, doi: 10.1016/j.seppur.2012.12.016.

[85] M. Yi *et al.*, "Zwitterion–Ag Complexes That Simultaneously Enhance Biofouling Resistance and Silver Binding Capability of Thin Film Composite Membranes," *ACS Appl. Mater. Interfaces*, vol. 11, no. 17, pp. 15698–15708, May 2019, doi: 10.1021/acsami.9b02983.